

Sterile Neutrino Dark Matter and Leptogenesis in Left-Right Higgs Parity

David Dunsky^{1,2} Lawrence J. Hall^{1,2} Keisuke Harigaya³

¹*Department of Physics, University of California, Berkeley, California 94720, USA*

²*Theoretical Physics Group, Lawrence Berkeley National Laboratory, Berkeley, California 94720, USA*

³*School of Natural Sciences, Institute for Advanced Study, Princeton, New Jersey 08540, USA*

ABSTRACT: The standard model Higgs quartic coupling vanishes at $(10^9 - 10^{13})$ GeV. We study $SU(2)_L \times SU(2)_R \times U(1)_{B-L}$ theories that incorporate the Higgs Parity mechanism, where this becomes the scale of Left-Right symmetry breaking, v_R . Furthermore, these theories solve the strong CP problem and predict three right-handed neutrinos. We introduce cosmologies where $SU(2)_R \times U(1)_{B-L}$ gauge interactions produce right-handed neutrinos via the freeze-out or freeze-in mechanisms. In both cases, we find the parameter space where the lightest right-handed neutrino is dark matter and the decay of a heavier one creates the baryon asymmetry of the universe via leptogenesis. A theory of flavor is constructed that naturally accounts for the lightness and stability of the right-handed neutrino dark matter, while maintaining sufficient baryon asymmetry. The dark matter abundance and successful natural leptogenesis require v_R to be in the range $(10^{10} - 10^{13})$ GeV for freeze-out, in remarkable agreement with the scale where the Higgs quartic coupling vanishes, whereas freeze-in requires $v_R \gtrsim 10^9$ GeV. The allowed parameter space can be probed by the warmness of dark matter, precise determinations of the top quark mass and QCD coupling by future colliders and lattice computations, and measurement of the neutrino mass hierarchy.

Contents

1	Introduction	2
2	Higgs Parity	4
2.1	Vanishing quartic	4
2.2	Left-right Higgs Parity	5
2.3	Strong CP problem	6
2.4	Prediction for the Higgs Parity symmetry breaking scale	6
3	Right-handed neutrino dark matter	7
3.1	Neutrino masses	8
3.2	The lightest right-handed neutrino as dark matter	8
4	Cosmological production of right-handed neutrino dark matter	9
4.1	Relativistic freeze-out and dilution	9
4.2	Freeze-in	12
5	Leptogenesis from heavy right-handed neutrino decay	13
5.1	The baryon asymmetry in freeze-out and freeze-in cosmologies	13
5.2	Enhancing the lepton asymmetry parameter	16
5.3	Restriction on neutrino masses in freeze-in cosmology	18
6	Naturalness and radiative corrections in the effective field theory	19
6.1	Conventional LR symmetric theories	20
6.2	Left-right Higgs Parity	21
7	A UV Completion yielding a light, long-lived N_1	23
7.1	The UV completion: tree-level	24
7.2	The UV completion: quantum corrections	25
7.2.1	Corrections from lepton Yukawas	25
7.2.2	Corrections from charged fermion Yukawa couplings	28
8	Natural leptogenesis	31
8.1	Models for enhanced asymmetry parameter	31
8.2	Radiative corrections: N_1 lifetime	32
8.3	Natural leptogenesis for freeze-out cosmology	34
8.4	Natural leptogenesis for freeze-in cosmology	36
9	Conclusions and discussion	39

1 Introduction

The discovery at the Large Hadron Collider of a Higgs boson with mass 125 GeV [1, 2] suggests a new paradigm for particle physics: the mass scale of new physics beyond the Standard Model (SM) is the scale where the Higgs quartic coupling vanishes, $\Lambda_{NP} \sim (10^9 - 10^{13})$ GeV, and not the weak scale. In this case, a variety of precision measurements at colliders, searches for rare processes, and cosmological observations could reveal this new physics. Λ_{NP} may be the scale where new symmetries emerge, for example Peccei-Quinn symmetry [3] or supersymmetry [4–7].

In this paper we study a Higgs Parity extension of the SM [8]. The $SU(2)$ gauge group is extended to $SU(2) \times SU(2)'$ and the Higgs sector is extended to $H(2, 1) + H'(1, 2)$, with a parity interchanging these Higgs multiplets, $H(2, 1) \leftrightarrow H'(1, 2)$. This Higgs Parity is spontaneously broken at Λ_{NP} by $\langle H' \rangle$, yielding the SM as the low energy effective theory. Remarkably, in the limit that the weak scale is far below Λ_{NP} , the Higgs quartic coupling is found to vanish at Λ_{NP} . One possibility is that $SU(2)'$ is part of a mirror sector, with mirror matter heavier than ordinary matter by a factor $\langle H' \rangle / \langle H \rangle$. This yields a highly predictive scheme for dark matter composed of mirror electrons [9, 10].

The most economical version of Higgs Parity, which we study in this paper and review in Sec. 2, is based on the simple extension of the SM electroweak gauge group to $SU(2)_L \times SU(2)_R \times U(1)_{B-L}$, first introduced in the 1970s [11–13]. We introduce Higgs doublet multiplets, $H_L(2, 1) + H_R(1, 2)$, rather than the conventional case of weak triplets and a $(2, 2)$ multiplet. Higgs Parity is imposed, $H_L(2, 1) \leftrightarrow H_R(1, 2)$, and spontaneously broken by $\langle H_R \rangle = v_R$, so that the SM Higgs quartic coupling vanishing at this Left-Right (LR) symmetry breaking scale v_R . This theory has the same number of gauge couplings and charged fermion Yukawa couplings as the SM. The Higgs potential has three parameters rather than two; but one of these is irrelevant as it only determines the mass of the right-handed Higgs boson. Another determines the electroweak scale $\langle H_L \rangle = v$, while the third provides a correlation between the Higgs boson mass, the top quark mass, the QCD coupling and v_R . For this theory, precision measurements at future colliders will play a key roll in sharpening this prediction for v_R , which is presently highly uncertain

$$v_R \sim (10^9 - 10^{13}) \text{ GeV}. \quad (1.1)$$

This will test whether precision gauge coupling unification in $SO(10)$ can be realized, and whether proton decay is within reach of future searches [14].

It has been known for many years that spacetime parity can solve the strong CP problem, in particular in the context of the gauge group $SU(2)_L \times SU(2)_R \times U(1)_{B-L}$ broken solely by doublets $H_{L,R}$ [15]. Indeed, the Higgs Parity theory we study actually has one less relevant parameter than the SM, since $\bar{\theta} = 0$ at tree-level. Non-zero contributions arise at the two-loop level and are estimated to typically generate the neutron electric dipole moment of order 10^{-27} ecm [8], and may be within the reach of current searches. Given the simplicity of the parity solution of the strong CP problem proposed in [15], why does the solution involving

an anomalous Peccei-Quinn symmetry [16, 17] dominate the literature? The answer may be that it requires an axion [18, 19]; a candidate for the cosmological dark matter with plausible production mechanisms [20–27]. Furthermore, the axion can be searched for in many ways and will be probed in the coming decade over much of its parameter range. In Secs. 3 and 4 of this paper, we show that the LR Higgs Parity theory also contains a dark matter candidate that can be produced in the early universe, leading to constraints and tests on the theory.

The minimal description of neutrino masses is to add the dimension 5 operator $\ell_i \ell_j H H$ to the SM, where ℓ_i are the lepton doublets and H the Higgs doublet. Alternatively, right-handed neutrinos N_i can be added to the theory together with the two operators

$$\mathcal{L}_{\text{SM+N}} \supset y_{ij} \ell_i N_j H + \frac{M_{ij}}{2} N_i N_j, \quad (+ \ell_i \ell_j H H) \quad (1.2)$$

involving two flavor flavor matrices. (The $\ell_i \ell_j H H$ operator could also be present, but in the seesaw mechanism [28–31] it is taken to be subdominant.) A virtue of adding the right-handed neutrinos is that, if they are produced in the early universe, their decays can lead to the cosmological baryon asymmetry via leptogenesis [32].

Theories containing $SU(2)_L \times SU(2)_R$ gauge symmetry necessarily contain N_i as the neutral member of the $SU(2)_R$ doublets $\bar{\ell}_i$. In the effective theory below the scale v_R , the generic structure of the operators leading to neutrino masses is

$$\mathcal{L}_{\text{LR}} \supset y_{ij} \ell_i N_j H_L + \frac{M_{ij}}{2} N_i N_j + c \frac{M_{ij}}{2v_R^2} \ell_i \ell_j H_L H_L. \quad (1.3)$$

Even though there are three operators, the flavor matrices for the $\ell_i \ell_j$ and $N_i N_j$ terms are identical, although there is a model dependent coefficient c in the relative strengths of these two terms. If the lightest right-handed neutrino N_1 has a very small mass M_1 , it could be dark matter, produced in the early universe via $SU(2)_R \times U(1)_{B-L}$ gauge interactions [33–35]. With an abundance set by freeze-out (and subsequent dilution by the decay of a heavier right-handed neutrino, N_2) the allowed range of the (M_1, v_R) parameter space was found to be restricted to a triangle, with a location that depended on c [35]. With $c = 1$, the allowed ranges within the triangle were roughly $M_1 \sim 2 - 300$ keV and $v_R \sim 10^{10 \pm 2}$ GeV. Lowering c led to a lowering of v_R and a reduction in the range for M_1 , with no parameter space for $v_R < 10^6$ GeV. Increasing c above unity requires fine-tuning in the theory, but opens up regions to larger values of M_1 and v_R . Large values of these parameters were also consistent with N_1 dark matter produced via freeze-in.

In the LR Higgs Parity theory, neutrino masses are generated by the operators of (1.3) with $c = 1$. As noted above, without interactions for neutrino masses the LR Higgs Parity theory has one fewer relevant parameter than the SM; adding the neutrino mass interactions, (1.2) for the SM and (1.3) with $c = 1$ for Higgs Parity, does not alter this. Thus N_1 dark matter can arise as in [35] and, remarkably, in the case that its abundance is determined by freeze-out, the required scale $v_R \sim 10^{10 \pm 2}$ GeV lies inside the range (1.1) determined by the Higgs mass. N_1 dark matter can be probed by future precision collider data that tightens the range of (1.1).

In Sec. 5 we show that leptogenesis from the decay of N_2 is possible in this theory, at the same time that N_1 provides the dark matter, and we investigate the extent to which the resulting reduced range for M_1 can be probed using 21cm cosmology.

In theories of sterile neutrino dark matter, there are naturalness issues for the small mass and long lifetime of the sterile neutrino. This is especially true in the LR symmetric theory, as the interactions of N_i are either determined by symmetry or constrained by the observed neutrino masses and mixings. In Sec. 6 we study radiative corrections to the mass and lifetime in the effective theory where quark and lepton masses arise from dimension 5 operators. These lead to significant naturalness constraints on the parameter space for dark matter. In Sec. 7 we introduce UV completions of these operators that greatly improve the naturalness of the long-lived, light right-handed neutrino dark matter. In Sec. 8 we study the naturalness of leptogenesis in these theories and find highly restricted ranges for the LR symmetry breaking scale, v_R , and the dark matter mass, M_1 . Conclusions are drawn in Sec. 9.

2 Higgs Parity

We begin with a brief review of Higgs Parity, first introduced in [8], as a model that simultaneously predicts a nearly vanishing Higgs quartic coupling at a scale 10^{9-13}GeV and solves the strong CP problem.

2.1 Vanishing quartic

Higgs Parity is a Z_2 symmetry that exchanges the $SU(2)_L$ gauge interaction with a new $SU(2)'$ interaction. The SM Higgs field $H(2, 1)$ is exchanged with its Z_2 partner $H'(1, 2)$, where the brackets show the $(SU(2)_L, SU(2)')$ charges. The scalar potential of H and H' is

$$V(H, H') = -m^2 (|H|^2 + |H'|^2) + \frac{\lambda}{2} (|H|^2 + |H'|^2)^2 + \lambda' |H|^2 |H'|^2. \quad (2.1)$$

We assume that the mass scale m is much larger than the electroweak scale, v .

With positive m^2 , H' obtains a large vacuum expectation value $\langle H' \rangle = m/\lambda^{1/2} \equiv v'$ and Higgs Parity is spontaneously broken. After integrating out H' at tree-level, the low energy effective potential of H is

$$V_{\text{LE}}(H) = \lambda' v'^2 |H|^2 - \lambda' \left(1 + \frac{\lambda'}{2\lambda}\right) |H|^4. \quad (2.2)$$

The hierarchy $v \ll v'$ is obtained only if the quadratic term is small, which requires a small value of $\lambda' \sim -v^2/v'^2$. The quartic coupling of the Higgs H , λ_{SM} , is then very small at the symmetry breaking scale v' . The nearly vanishing quartic coupling can be understood by an approximate global $SU(4)$ symmetry under which (H, H') forms a fundamental representation. For $|\lambda'| \ll 1$ the potential in Eq. (2.1) becomes $SU(4)$ symmetric. The $SU(4)$ symmetry is spontaneously broken by $\langle H' \rangle$ and the SM Higgs is understood as a Nambu-Goldstone boson with vanishing potential.

At tree-level the potential still leads to $\langle H \rangle = \langle H' \rangle = v'/\sqrt{2}$ because of the small quartic coupling. However, for extremely small λ' , vacuum alignment in the $SU(4)$ space is fixed by quantum corrections which violate the $SU(4)$ symmetry. The dominant effect is renormalization group running from energy scale v' down to v . The top contribution dominates over the gauge contribution and generates a positive quartic coupling $\lambda_{\text{SM}}(v) \simeq 0.1$, and creates the minimum of the potential at $v \ll v'$. From the perspective of running from low to high energy scales, the scale at which the SM Higgs quartic coupling nearly vanishes is the scale v' . Threshold corrections to $\lambda_{\text{SM}}(v')$ are computed in [9, 14] and are typically $O(10^{-3})$.

The vacuum alignment can be also understood in the following way. For $\lambda' > 0$, the minima of the potential are $(\langle H \rangle, \langle H' \rangle) = (v', 0)$ and $(0, v')$, where $v' \equiv m/\lambda^{1/2}$, and the mass of Higgses are as large as m . For $\lambda' < 0$, the minima are $\langle H \rangle = \langle H' \rangle \sim v'$. None of the minima for $\lambda > 0$ and $\lambda' < 0$ has a non-zero but small v . To obtain a viable vacuum, we need $\lambda' \simeq 0$, for which the potential has an accidental $SU(4)$ symmetry and nearly degenerate vacua with $\langle H^2 \rangle + \langle H'^2 \rangle = v'^2$. In this case, quantum corrections must be taken into account to determine the minimum. The dominant effect is given by the top quark Yukawa coupling. The Coleman-Weinberg potential given by the top Yukawa makes $(\langle H \rangle, \langle H' \rangle) = (v', 0)$ and $(0, v')$ minima. By switching-on small negative λ' , the vacuum $(\langle H \rangle, \langle H' \rangle) = (0, v')$ is slightly destabilized and we may obtain $(\langle H \rangle, \langle H' \rangle) = (v, v')$ with $v \ll v'$. There also is a physically equivalent minimum connected to this by Higgs Parity, $(\langle H \rangle, \langle H' \rangle) = (v', v)$.

2.2 Left-right Higgs Parity

In this work, we consider the case where only the right-handed (SM) fermions are charged under $SU(2)'$, i.e., $SU(2)_R$, and we accordingly relabel (H, H') as (H_L, H_R) . The gauge group of the theory is $SU(3)_c \times SU(2)_L \times SU(2)_R \times U(1)_{B-L}$ and the matter content is listed in Table 1. The presence of the right-handed neutrinos is now required by the gauge symmetry. Higgs Parity maps $SU(2)_L \leftrightarrow SU(2)_R$, and hence $\ell \leftrightarrow \bar{\ell}^\dagger$, $q \leftrightarrow \bar{q}^\dagger$, and $H_L \leftrightarrow H_R^\dagger$.¹ The symmetry breaking pattern is,

$$SU(3)_c \times SU(2)_L \times SU(2)_R \times U(1)_{B-L} \times Z_2 \xrightarrow{\langle H_R \rangle} SU(3)_c \times SU(2)_L \times U(1)_Y \xrightarrow{\langle H_L \rangle} SU(3)_c \times U(1)_{\text{EM}}. \quad (2.3)$$

In contrast to conventional Left-Right symmetric models, we do not introduce scalar multiplets in $(2, 2)$, $(3, 1)$ or $(1, 3)$ representations of $SU(2)_L \times SU(2)_R$ around the scale v_R ; the Higgs Parity explanation for the vanishing quartic coupling holds only if $SU(2)_R$ and $SU(2)_L$ symmetry are dominantly broken by H_R and H_L . Thus, Yukawa couplings are forbidden at the renormalizable level, and arise from dimension-5 operators,

$$-\mathcal{L}_{e,u,d} = \frac{c_{ij}^u}{M} q_i \bar{q}_j H_L H_R + \frac{c_{ij}^d}{M} q_i \bar{q}_j H_L^\dagger H_R^\dagger + \frac{c_{ij}^e}{M} \ell_i \bar{\ell}_j H_L^\dagger H_R^\dagger + \text{h.c.}, \quad y_{ij}^f \equiv c_{ij}^f \frac{v_R}{M} \quad (2.4)$$

$$-\mathcal{L}_{\nu,N} = \frac{c_{ij}}{2M} (\ell_i \ell_j H_L H_L + \bar{\ell}_i \bar{\ell}_j H_R H_R) - \frac{b_{ij}}{M} \ell_i \bar{\ell}_j H_L H_R + \text{h.c.} \quad y_{ij} \equiv b_{ij} \frac{v_R}{M} \quad (2.5)$$

¹If the Z_2 does not include spacetime parity, $\ell \leftrightarrow \bar{\ell}$, $q \leftrightarrow \bar{q}$ and $H_L \leftrightarrow H_R$

	q	ℓ	$\bar{q} = (\bar{u}, \bar{d})$	$\bar{\ell} \equiv (N, \bar{e})$	H_L	H_R
$SU(3)_c$	3	1	$\bar{3}$	1	1	1
$SU(2)_L$	2	2	1	1	2	1
$SU(2)_R$	1	1	2	2	1	2
$U(1)_{B-L}$	1/6	-1/2	-1/6	1/2	1/2	-1/2

Table 1. The gauge charges of quarks, leptons, H_L , and H_R .

These can arise, e.g., from exchanges of massive Dirac fermions (as considered in [8, 14]) or from the exchange of a massive scalar with a charge $(1, 2, 2, 0)$.² In Sec. 7, we take some of the masses of the Dirac fermions to be small. In this case, the corresponding SM right-handed fermions dominantly come from the Dirac fermions rather than the $SU(2)_R$ doublets. The origin of the neutrino masses are discussed in Sec. 3.

2.3 Strong CP problem

Higgs Parity can also solve the strong CP problem if $SU(3)_c$ is Z_2 neutral and the Z_2 symmetry includes space-time parity [8]. Then spacetime parity forbids the QCD θ parameter at tree-level and requires the quark mass matrices $y_{ij}^f v$ in Eq. (2.4) to be Hermitian and thus enjoy real eigenvalues. The determinant of the quark mass matrix is then real and hence $\bar{\theta}$ is absent at both tree-level and at one-loop. Two-loop corrections to the quark mass matrix give non-zero $\bar{\theta}$ [8], but can be below the experimental upper bound from the neutron electric dipole moment.

Solving the strong CP problem by restoring space-time parity was first pointed out in [36, 37]. The first realistic model was proposed in [15, 40], which used $(2, 1) + (1, 2)$ Higgses and Dirac fermions to generate the Yukawa coupling in Eq. (2.4). In their model, space-time parity is assumed to be softly broken in the Higgs potential to obtain the hierarchy $v \ll v_R$. In the setup of [8], Higgs Parity including space-time parity is spontaneously broken without soft breaking and predicts vanishing $\lambda_{SM}(v_R)$. The embedding of the theory into $SO(10)$ unification is achieved in [8, 14], with Higgs Parity arising from a Z_2 subgroup of $SO(10)$.

2.4 Prediction for the Higgs Parity symmetry breaking scale

Between the electroweak scale and the Left-Right scale v_R , the running of the Higgs quartic coupling λ_{SM} is exactly the same as in the SM. We follow the computation in [41] and show the running in the left panel of Fig. 1 for a range of values for the top quark mass $m_t = (173.0 \pm 0.4)$ GeV, QCD coupling constant at the Z boson mass $\alpha_S(m_Z) = (0.1181 \pm 0.0011)$, and Higgs mass $m_h = (125.18 \pm 0.16)$ GeV.

²To obtain the up and down quark masses solely from the exchange of $(1, 2, 2, 0)$, it must be a complex scalar rather than a pseudo-real scalar. In this case, the strong CP problem cannot be solved by parity because of the complex vacuum expectation value of the complex scalar, unless extra symmetries, such as supersymmetry, are imposed [36–39].

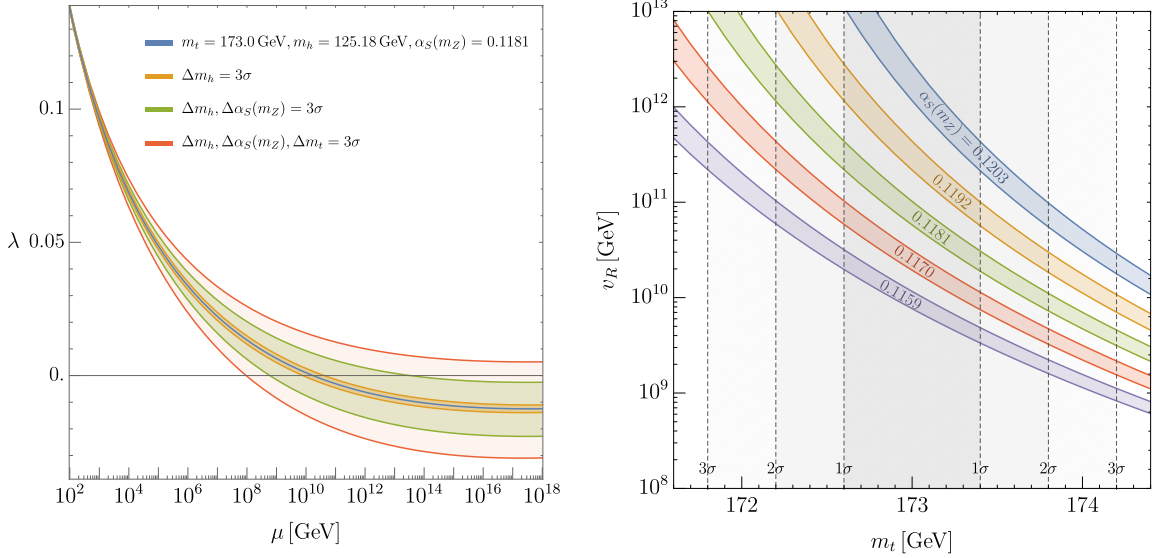


Figure 1. (Left) Running of the SM quartic coupling. (Right) Predictions for the scale v_R as a function of the top quark mass, m_t . Contours of $\alpha_S(M_Z)$ show how the prediction changes with the uncertainty in the QCD coupling constant. The thickness of each countour corresponds to $\pm 1\sigma$ deviation in m_h .

The value of the SM quartic coupling at the scale v_R is not exactly zero because of the threshold correction [9],

$$\lambda_{\text{SM}}(v_R) \simeq -\frac{3}{8\pi^2} y_t^4 \ln \frac{e}{y_t} + \frac{3}{128\pi^2} (g^2 + g'^2)^2 \left(\ln \frac{e\sqrt{2}}{\sqrt{g^2 + g'^2}} - \ln \frac{g^2}{\sqrt{g^4 - g'^4}} \right) + \frac{3}{64\pi^2} g^4 \ln \frac{e\sqrt{2}}{g}, \quad (2.6)$$

where the $\overline{\text{MS}}$ scheme is assumed. The prediction for the scale v_R is shown in the right panel of Fig. 1 as a function of m_t . Colored contours show how the prediction in v_R changes when the QCD coupling constant varies by ± 2 deviations about its mean, $\alpha_S(M_Z) = 0.1181 \pm 0.0011$. The thickness of each curve corresponds to the 1-sigma uncertainty in the measured Higgs mass, $m_h = (125.18 \pm 0.16)$ GeV. With 2σ uncertainties, v_R can be as low as 10^9 GeV. Future measurements of SM parameters can pin down the scale v_R with an accuracy of a few tens of percent [9].

3 Right-handed neutrino dark matter

In this section, we review the results of [35] on the general properties and constraints of right-handed neutrino dark matter in LR theories.

3.1 Neutrino masses

The effective Lagrangian of (2.5) leads to a 6×6 neutrino mass matrix,

$$\begin{pmatrix} \nu_i & N_i \end{pmatrix} \begin{pmatrix} M_{ij} v^2/v_R^2 & y_{ij}v \\ y_{ji}v & M_{ij}^{(*)} \end{pmatrix} \begin{pmatrix} \nu_j \\ N_j \end{pmatrix}, \quad (3.1)$$

where $M_{ij} = c_{ij}v_R^2/M$. Without loss of generality, we can work in a basis where c_{ij} is diagonal such that

$$M_{ij} = M_i \delta_{ij}, \quad (3.2)$$

with all M_i real and positive. Upon integrating out the three heavy states, we obtain a mass matrix for the three light neutrinos:

$$m_{ij} = \delta_{ij} \frac{v^2}{v_R^2} M_i - y_{ik}v \frac{1}{M_k} y_{jk}v \equiv \delta_{ij} m_i^{(5)} - m_{ij}^{(ss)}. \quad (3.3)$$

In this basis, and in the limit that y_{ij} is diagonal, the lepton flavor mixing arises entirely from the charged lepton mass matrix.

3.2 The lightest right-handed neutrino as dark matter

We define N_1 as the right-handed neutrino responsible for the dark matter (DM) density of the universe.³ Even though there is no symmetry that stabilizes N_1 , it may be sufficiently long-lived to be a DM candidate.

N_1 decays via $N_1 - \nu$ mixing controlled by y_{i1} . The $N_1 - \nu$ mixing angle is given by

$$\sin 2\theta_1 \equiv \frac{v}{M_1} \sqrt{\sum_i |y_{i1}|^2}, \quad (3.4)$$

where $v \simeq 174$ GeV. The experimental constraints on $\sin 2\theta_1$ arise from two different processes: 1) N_1 DM may be overproduced via the Dodelson-Widrow mechanism [42]. 2) N_1 DM decays into $\nu\gamma$ and may overproduce photons relative to observed diffuse photon backgrounds and galaxy fluxes [43]. This decay rate is given by:

$$\Gamma_{N_1 \rightarrow \nu\gamma} \simeq \frac{9\alpha}{8192\pi^4} \frac{M_1^5}{v^4} \sin^2 2\theta_1 \simeq (1.5 \times 10^{30} \text{ sec})^{-1} \left(\frac{M_1}{1 \text{ keV}} \right)^5 \left(\frac{\sin^2 2\theta_1}{5 \times 10^{-9}} \right). \quad (3.5)$$

These two constraints are summarized by the experimental limit on the mixing angle [43],

$$\frac{v^2}{M_1^2} \sum_i |y_{i1}|^2 \leq \sin^2 2\theta_{1\text{exp}} \simeq 5 \times 10^{-9} \begin{cases} \left(\frac{M_1}{3 \text{ keV}} \right)^{-1.8} \times D & \text{(Overproduction)} \\ \left(\frac{M_1}{3 \text{ keV}} \right)^{-5} & \text{(Decay)}. \end{cases} \quad (3.6)$$

³Note that our numbering of SM neutrinos does not necessarily coincide with the neutrino numbering commonly found in the literature.

Here D is a possible dilution factor after N_1 is produced by the Dodelson-Widrow mechanism. The higher photometric sensitivities of next generation x-ray and gamma-ray telescopes such as ATHENA [44] and e-ASTROGAM [45] may probe an order of magnitude smaller decay rate [46]. For $M_1 > 1$ MeV, the tree-level decay $N_1 \rightarrow e^+e^-\nu$ is open and the resultant constraint on y_{i1} is similar to (3.6).

Regardless of how small y_{i1} is, constraints arise from N_1 decays mediated by gauge exchange. For example, N_1 decays into $\ell^\pm + \text{hadron(s)}$ via W_R exchange when kinematically allowed. In addition, W_R and W_L mix with each other by a top-bottom-loop, and N_1 may decay into $\ell^+\ell^-\nu$. The experimental upper bounds on these decay rates are about $10^{-25} \text{ sec}^{-1}$ [47]. Furthermore, the $W_R - W_L$ mixing also generates a radiative decay of N_1 into $\nu\gamma$ [34, 48, 49], which has a stronger experimental upper limit of about $10^{-27} \text{ sec}^{-1}$ due to the emission of a hard photon [43]. The parameter region with large M_1 and/or small v_R is excluded by these gauge-induced decays as discussed more in [35] and shown graphically in Fig. 3.

4 Cosmological production of right-handed neutrino dark matter

In this section, we review the two production mechanisms of N_1 DM considered in this paper [35]:

- At sufficiently high reheating temperatures $T_{\text{RH}}^{\text{inf}}$ after inflation, N_i have a thermal abundances from W_R exchange. The N_1 abundance is reduced by an appropriate amount to the DM abundance by making N_2 long-lived so that entropy is produced upon decaying.
- At low reheating temperatures $T_{\text{RH}}^{\text{inf}}$ after inflation, the N_1 DM abundance is produced by freeze-in via W_R exchange. N_2 are also produced by freeze-in, via W_R exchange or via the Yukawa couplings with ℓH .

In these two scenarios, N_1 DM can be obtained over a wide range of parameter space.

4.1 Relativistic freeze-out and dilution

The right-handed neutrinos couple to the SM bath via W_R exchange. If the reheat temperature of the universe after inflation is sufficiently high,

$$T_{\text{RH}}^{\text{inf}} \gtrsim 10^8 \text{ GeV} \left(\frac{v_R}{10^{10} \text{ GeV}} \right)^{4/3}, \quad (4.1)$$

the right-handed neutrinos reach thermal equilibrium and subsequently decouple with a thermal yield $Y_{\text{therm}} \simeq 0.004$.⁴ For N_1 to have the observed DM abundance requires $m_{N_1} \simeq 100$ eV. Such light sterile neutrino DM, however, is excluded by the Tremaine-Gunn [50–52] and warmness [53–56] bounds; see [43] for a recent review.

⁴The analysis in this section is also applicable to lower $T_{\text{RH}}^{\text{inf}}$ as long as N_1 and N_2 are frozen-in from W_R exchange, and N_1 is overproduced as DM (see Eq. (4.7)). In such a scenario, the required dilution to realize N_1 DM is diminished, and hence the warmness constraints on N_1 slightly increase above 2 keV. See Fig. 3 for the warmness constraints on a pure freeze-in cosmology without any dilution.

N_1 may be DM if their abundance is diluted. If another right-handed neutrino, N_2 , is sufficiently long-lived such that it comes to dominate the energy density of the universe and produces entropy when it decays, it can dilute the DM abundance and cool N_1 below warmness bounds [34, 57]. The relic density of N_1 is

$$\begin{aligned} \frac{\rho_{N_1}}{s} &= 1.6 \frac{3}{4} \frac{M_1}{M_2} T_{\text{RH}}, \\ \Rightarrow \frac{\Omega_{N_1}}{\Omega_{\text{DM}}} &\simeq \left(\frac{M_1}{10 \text{ keV}} \right) \left(\frac{300 \text{ GeV}}{M_2} \right) \left(\frac{T_{\text{RH}}}{10 \text{ MeV}} \right), \end{aligned} \quad (4.2)$$

where the numerical factor 1.6 is taken from [58], ρ_{N_1} is the energy density, s is the entropy density, $\Omega_{\text{DM}} \simeq 0.25$ is the observed cosmic relic abundance, and T_{RH} is the decay temperature of N_2 , as set by its total decay rate Γ_{N_2}

$$T_{\text{RH}} = \left(\frac{10}{\pi^2 g_*} \right)^{1/4} \sqrt{\Gamma_{N_2} M_{\text{Pl}}}. \quad (4.3)$$

The reheating bound from hadronic decays of N_2 during BBN ($T_{\text{RH}} > 4 \text{ MeV}$) [59–61], requires that N_2 is heavy enough,

$$M_2 \gtrsim 24 \text{ GeV} \frac{M_1}{2 \text{ keV}}. \quad (4.4)$$

Low reheating temperatures can also affect the CMB since some decays occur after neutrinos decouple and heat up only electrons and photons, relatively cooling neutrinos and reducing the effective number of neutrinos [59, 60, 62]. In our case, N_2 also decays into neutrinos and the bound from the CMB, $T_{\text{RH}} > 4 \text{ MeV}$ [63], may be relaxed.

To achieve the dilution of N_1 dark matter, N_2 must be long-lived enough. N_2 can always beta decay through W_R exchange into right-handed fermions, $N_2 \rightarrow (\ell^+ \bar{u} d, \ell^- u \bar{d})$ and $N_2 \rightarrow N_1 \ell^+ \ell^-$. These decay channels are unavoidable as they are independent of the free-parameter y_{i2} , and prevent N_2 from efficiently diluting N_1 for large M_2 and/or small v_R . In addition, N_2 can decay through the couplings y_{i2} . When $M_2 \gtrsim v$, N_2 can decay at tree-level via $N_2 \rightarrow \nu h, \nu Z, \ell^\pm W_L^\mp$ while for $M_2 \lesssim v$, N_2 can beta decay through W_L/Z exchange and active-sterile mixing to SM fermions, $N_2 \rightarrow \ell u d, \ell^+ \ell^- \nu, \nu \nu \bar{\nu}$. As discussed in more detail in Ref. [35], these decays require y_{i2} to be sufficiently small.

In Ref. [35], we used the above results, together with the radiative stability bound on N_1 , to derive constraints on the neutrino mass matrix of (3.3). We considered the cases with $M_3 \gtrsim M_2$ and $M_3 \ll M_2$. As we will see later, efficient leptogenesis require that $M_3 \gtrsim M_2$. For this case, Ref. [35] shows that the lightest neutrino mass eigenstate is closely aligned with ν_1 and has a mass $m_1 \ll \sqrt{\Delta m_{\text{sol}}^2}$. The other two mass eigenstates are very close to ν_2 and ν_3 and have masses $m_2 = (v^2/v_R^2)M_2$ and $m_3 = (v^2/v_R^2)M_3 - y_{33}^2 v^2/M_3$. The mass of N_2 is thus fixed as

$$M_2 \simeq m_2 \left(\frac{v_R}{v} \right)^2. \quad (4.5)$$

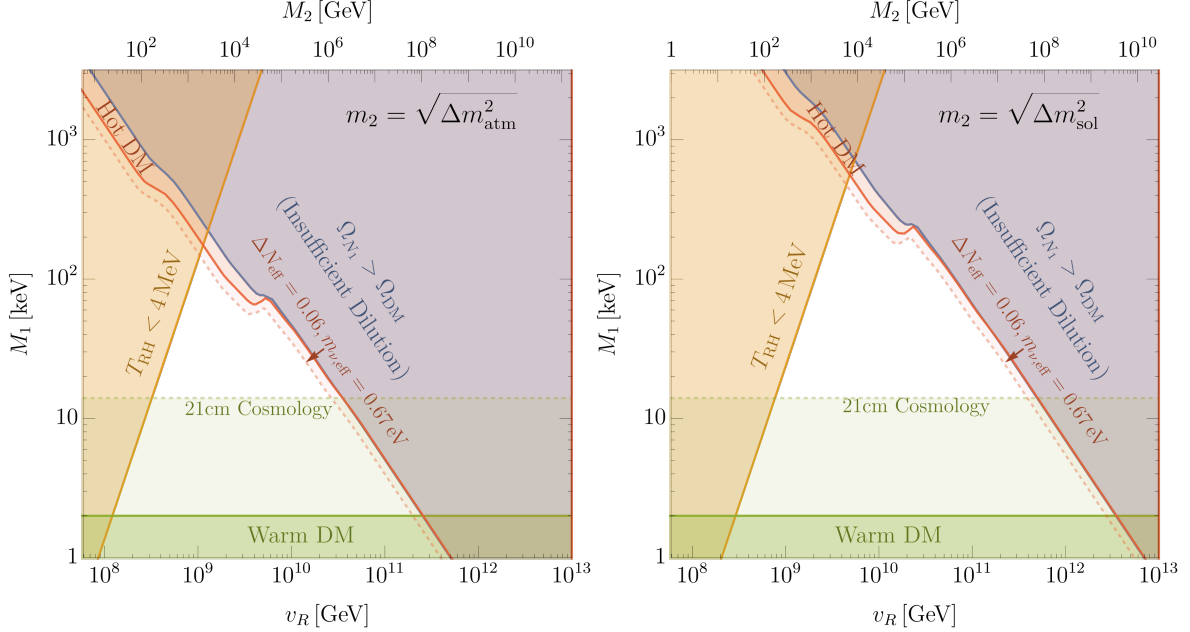


Figure 2. The parameter space of N_1 DM produced by relativistic freeze-out and dilution from N_2 decay in terms of the Left-Right symmetry breaking scale, v_R , and the mass of N_1 , M_1 . We show constraints from N_2 decaying after Big Bang Nucleosynthesis (orange), decaying too early to provide sufficient N_1 dilution (blue), warm DM bounds (green), and hot DM bounds (red). In addition we show prospects of improved searches for hot DM from CMB telescopes (dashed red), and warm DM from 21-cm cosmology (dashed green). We fix the ν_2 mass with the atmospheric neutrino mass difference, $m_2 = \sqrt{\Delta m_{\text{atm}}^2}$, **left**, and the solar neutrino mass difference, $m_2 = \sqrt{\Delta m_{\text{sol}}^2}$, **right**.

In Fig. 2, we show the constraints on (v_R, M_1) when $m_2 = \sqrt{\Delta m_{\text{atm}}^2}$ (**left**) and $m_2 = \sqrt{\Delta m_{\text{sol}}^2}$ (**right**). In the orange shaded region, the required T_{RH} is below 4 MeV, which is excluded by hadronic decays of N_2 during BBN [59, 60]. The green-shaded region is excluded due to the warmness of N_1 affecting large scale structure [53–56]. The light green-shaded region shows the sensitivity of future observations of 21cm lines [64]. In the blue-shaded region, N_2 decays too quickly through W_R exchange to efficiently dilute the N_1 energy density. The non-trivial shape of the blue-shaded region is due to the T_{RH} dependent effective degrees of freedom.

The blue line itself is an interesting region of parameter space, which does not require any tuning but simply corresponds to the limit where the dominant decay is set entirely by W_R exchange. In this limit, the N_1 abundance has two contributions: from N_2 decay through $N_2 \rightarrow N_1 \ell^+ \ell^-$ as well as the prior thermal abundance from relativistic decoupling. The former contribution makes up 10% of DM and is hot. The red-shaded region is excluded by the effect of the hot component on the CMB and structure formation, as set by current limits of ΔN_{eff} and $m_{\nu, \text{eff}}$ [65]. The low v_R part of the blue line is already excluded, and high v_R is in tension. CMB Stage IV experiments [66, 67] can cover the light red-shaded region and probe the limit where N_2 dominantly decays via the W_R exchange.

N_3 . These contributions, however, are always subdominant to the direct freeze-in production of N_1 , whether $N_{2,3}$ are produced by the W_R interaction or the ℓNH interaction.

The contours of Fig. 3 show the reheat temperature after inflation for N_1 DM to arise from freeze-in, in the (v_R, M_1) plane. In the green region, the warmth of N_1 affects large scale structure. Since N_1 from freeze-in are not diluted, they are warmer than N_1 from freeze-out and dilution, for a fixed M_1 . More concretely, the free-streaming length is larger by a factor of approximately $(4/3.2)(Y_{\text{therm}}M_1s/\rho_{\text{DM}})^{1/3}$, giving a commensurately stronger warm DM bound compared to Fig. 2. Here, the factor of $4/3.2$ comes from the difference in $\langle p/T \rangle$ between the non-thermal freeze-in and the thermal freeze-out distributions, as discussed in [68]. In the blue and pink regions, the decay of N_1 mediated by W_R or $W_R - W_L$ -mixing overproduces the observed amount of galactic gamma-rays, respectively [47]. Similarly, the decay of N_1 via active-sterile mixing overproduces the observed galactic x-rays and gamma-rays for the mixing angle $\sin^2 2\theta_1$ labeling the purple dotted contours. Unlike the W_R -mediated decay, which is fixed by v_R , the decay via $N_1 - \nu$ mixing is set by the free parameters y_{i1} .

Fig. 3 shows that the parameter space for N_1 DM from freeze-in is weakly constrained compared to that of N_1 DM from freeze-out and dilution, shown in Fig. 2. For example, v_R could be as low as about 100 TeV, with the reheat temperature after inflation below 100 GeV. Likewise, bounds on M_1 are weak; although, as M_1 increases, $\sin^2 2\theta_1$ is constrained to become extremely small to keep N_1 sufficiently long-lived. In the next section we find that, if leptogenesis via N_2 decay is incorporated into the N_1 DM freeze-in cosmology, the (M_1, v_R) parameter space becomes more tightly constrained.

5 Leptogenesis from heavy right-handed neutrino decay

In both the freeze-out and freeze-in cosmologies, where N_1 makes up DM, the decays of N_2 can produce a baryon asymmetry through leptogenesis. Producing a large enough lepton asymmetry requires N_3 to have a sizable Yukawa coupling y_{33} or y_{23} ; $y_{13} = y_{31}^*$ is small due to the longevity of N_1 . N_3 is therefore short-lived.

The lepton asymmetry yield from N_2 decay is

$$Y_L = \epsilon\eta Y_{\text{therm}}B \quad (5.1)$$

where ϵ is the asymmetry created per N_2 decay into ℓH_L or $\ell^\dagger H_L^\dagger$, η is the efficiency factor, and $B \equiv \text{Br}(N_2 \rightarrow \ell H_L) + \text{Br}(N_2 \rightarrow \ell^\dagger H_L^\dagger)$. In the next two sub-sections we discuss the abundance of N_2 , which differs in the two cosmologies, and the quantities ϵ and η .

5.1 The baryon asymmetry in freeze-out and freeze-in cosmologies

When the reheat temperatures after inflation, $T_{\text{RH}}^{\text{inf}}$, is high, N_1 DM is produced by freeze-out and subsequent dilution from N_2 decay. Although the initial N_2 abundance is thermal, the efficiency η is reduced by the dilution produced from N_2 . Also, if the reheat temperature after the N_2 MD-era, T_{RH} , is below the weak scale, the baryon asymmetry is reduced because

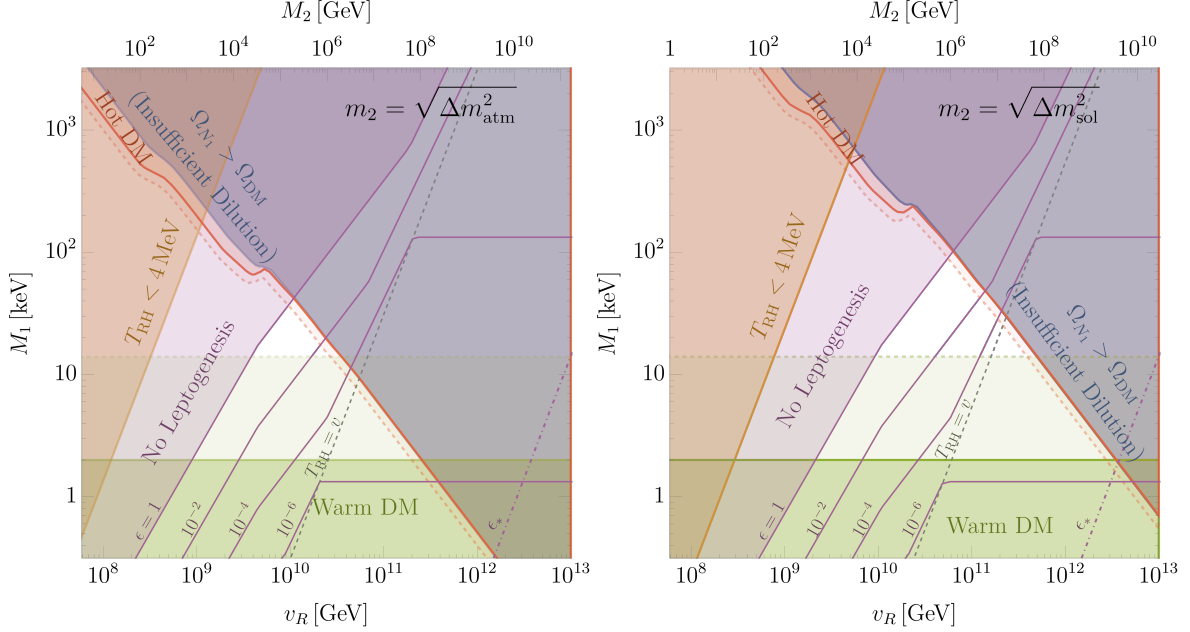


Figure 4. Purple contours of the asymmetry parameter, ϵ , required to produce the observed baryon asymmetry, $Y_B \simeq 8 \times 10^{-11}$ in the freeze-out cosmology. Larger values of ϵ are required as M_1 increases due to the greater dilution necessary to realize N_1 dark matter. Likewise, larger values of ϵ are required at low v_R when T_{RH} is below the weak scale, as indicated by the dashed gray line. In this regime, the baryon asymmetry is generated only by N_2 that decay at temperatures above the weak scale, where electroweak sphalerons are operative. To the left of the dot-dashed purple contour, the baryon asymmetry can only be realized when ϵ is greater than its natural maximum, ϵ_* .

only the lepton number produced above the weak scale is converted to baryons by sphaleron processes. The N_2 decays yield a baryon asymmetry

$$Y_B = \frac{28}{79} \epsilon \left(\frac{3T_{RH}}{4M_2} \right) f B = \frac{28}{79} \epsilon \left(\frac{\rho_{DM}/s}{M_1} \right) f B, \quad (\text{Freeze-Out} + \text{Dilution}) \quad (5.2)$$

where the factor of $28/79$ accounts for the conversion of the lepton asymmetry into the baryon asymmetry via sphaleron processes [69]. f is the fraction of decays that occur when the temperature of the universe is above the weak scale where sphalerons convert the lepton asymmetry into a baryon asymmetry. The fraction depends on whether the temperature of the universe falls below v during a radiation-dominated or N_2 matter-dominated era:

$$f = \Gamma_{N_2} t(T=v) \simeq \begin{cases} (T_{RH}/v)^2 & T_{MD} < v \\ (T_{RH}/v)^2 (v/T_{MD})^{1/2} & T_{NA} < v < T_{MD} \\ (T_{RH}/v)^4 & T_{RH} < v < T_{NA} \\ 1 & v < T_{RH}. \end{cases} \quad (5.3)$$

Here, $T_{MD} = \frac{4}{3} M_2 Y_{\text{therm}}$ is the temperature at the start of the adiabatic matter-dominated era, and $T_{NA} = (T_{MD} T_{RH}^4)^{1/5}$ is the temperature at the start of the non-adiabatic matter-

dominated era [70, 71]. Fig. 4 shows contours of ϵ required to produce the observed baryon asymmetry, $Y_B \simeq 8 \times 10^{-11}$, in the (v_R, M_1) plane. The contours zig-zag through the plane due to the era-dependent change in f , according to Eq. (5.3). For large v_R , the reheat temperature is high and N_2 always decays before the electroweak phase transition so that $f = 1$ and the required ϵ depends solely on M_1 . As T_{RH} drops below v , as indicated by the dashed gray line, f falls below unity and ϵ is suppressed.

In addition, there is no efficiency lost due to cancellations between the lepton asymmetry generated during production with the lepton asymmetry generated during decay, since the production of N_2 through W_R exchange does not generate any lepton asymmetry. Since y_{i2} are small, the wash-out effect is negligible. Finally, we use the DM abundance from (4.2) to obtain the final result.

Conversely, in the limit when the reheat temperature after inflation, $T_{\text{RH}}^{\text{inf}}$, is low, $N_{1,2}$ abundances are frozen-in and the resultant baryon asymmetry is

$$Y_B = \frac{28}{79} \epsilon \eta Y_{\text{therm}} B. \quad (\text{Freeze-In}) \quad (5.4)$$

Note that without a thermal abundance, the freeze-in yield of N_2 is too low to induce a matter-dominated era, so that no entropy is produced when N_2 decays; this accounts for the difference between Eq. (5.4) and (5.2). The efficiency factor, η , of N_2 is [72]

$$\eta Y_{\text{therm}} \simeq \begin{cases} Y_{W_R} + 0.03 \left(\frac{\tilde{m}_2}{10^{-4} \text{ eV}} \right) Y_{\text{therm}} & : \tilde{m}_2 < 10^{-3} \text{ eV (Weak Washout)} \\ 0.03 Y_{\text{therm}} \left(\frac{\tilde{m}_2}{10^{-2} \text{ eV}} \right)^{-1.16} & : \tilde{m}_2 > 10^{-3} \text{ eV (Strong Washout)} \end{cases} \quad (5.5)$$

where

$$\tilde{m}_2 \equiv \sum_i |y_{i2}|^2 v^2 / M_2. \quad (5.6)$$

In the weak washout regime, when $\tilde{m}_2 < 10^{-3}$ eV, N_2 decays out-of-equilibrium. Y_{W_R} is the freeze-in yield of N_2 from W_R exchange, where we have set $\eta \simeq 1$ again for this production mechanism. Since the freeze-in abundance of N_1 and N_2 via W_R exchange is identical, Y_{W_R} is simply

$$Y_{W_R} = \frac{\rho_{N_1}/s}{M_1} = \frac{\rho_{\text{DM}}/s}{M_1}. \quad (5.7)$$

In the strong washout regime, where Y_2 reaches Y_{therm} by the Yukawa coupling y_{i2} , N_2 is in thermal equilibrium when $T \sim M_2$, and the lepton asymmetry is washed-out until the Yukawa interaction is out-of-equilibrium, strongly reducing the efficiency of leptogenesis. The maximum possible ηY_{therm} for freeze-in is about $0.1 Y_{\text{therm}}$, which occurs when $\tilde{m}_2 \simeq 10^{-3}$ eV at the transition between the weak and strong washout regimes [72]. The leptogenesis CP

asymmetry parameter, defined by the difference between the branching ratio of N_2 into a lepton and an anti-lepton [73], is given in the limit that $y_{i1} \ll 1$ by

$$\epsilon = \frac{(y_{33} + y_{22})^2}{8\pi} \frac{\text{Im}(y_{23}^2)}{y_{22}^2 + |y_{32}|^2} g(x) = \frac{(y_{33} + y_{22})^2}{8\pi} g(x) \sin^2 \alpha \sin 2\beta, \quad x = \frac{M_3^2}{M_2^2}. \quad (5.8)$$

Since the Higgs Parity solution to the strong CP problem requires y_{ij} to be Hermitian, the heavy 2×2 space contains a single phase $y_{23} \equiv |y_{23}|e^{i\beta}$. Furthermore, we introduce an angle α defined by $|y_{23}|/y_{22} \equiv \tan \alpha$. The function $g(x)$ is [32, 74]

$$g(x) \equiv \sqrt{x} \left(\frac{1}{1-x} + 1 - (1+x) \log \left(\frac{1}{x} + 1 \right) \right), \quad (5.9)$$

and is much less than unity when M_3 and M_2 are disparate, near unity when M_3 and M_2 are comparable, and much greater than unity as M_3 and M_2 become degenerate.

It is possible to choose $y_{33}, M_3/M_2, \alpha$ and β to achieve a sufficiently large asymmetry per decay (5.8) for successful N_2 leptogenesis in both the freeze-out and freeze-in N_1 DM cosmologies. For freeze-out, the baryon asymmetry generated by N_2 , (5.2), can match the observed baryon asymmetry $Y_B \simeq 8 \times 10^{-11}$ everywhere in the unshaded region of Fig. 4. At larger values of v_R , $\epsilon \sim 10^{-5}$ is sufficient. However, at lower v_R as T_{RH} drops below the weak scale, larger values are needed, as shown by the purple contours, as only the fraction of N_2 decaying above v result in baryogenesis. At the lowest values of v_R that give N_1 dark matter, an insufficient baryon asymmetry is generated even if y_{33} becomes non-perturbative and $\epsilon = 1$, as shown by the shaded purple region of Fig. 4. In the case of freeze-in cosmology there is no dilution, so that the baryon asymmetry of (5.4) can successfully yield the observed asymmetry everywhere in Fig. 3, except in the region not shown at very low v_R where $T_{\text{RH}}^{\text{inf}} \ll v$.

5.2 Enhancing the lepton asymmetry parameter

For comparable M_2 and M_3 , $g(x) \sim 1$, and for large angles $\alpha, \beta \sim 1$, the asymmetry parameter is of order $(y_{33} + y_{22})^2/8\pi$. For the freeze-out cosmology, y_{22} is negligible, while for the freeze-in cosmology y_{22} is subject to the similar constraints as y_{33} . We thus focus on y_{33} in this subsection. The coupling y_{33} determines the size of the seesaw contribution to the ν_3 mass via

$$m_{33} = m_3^{(5)} - m_{33}^{(ss)} = \frac{v^2}{v_R^2} M_3 - \frac{y_{33}^2 v^2}{M_3} - \underbrace{\frac{y_{32}^2 v^2}{M_2}}_{< 10^{-3} \text{ eV}}. \quad (5.10)$$

In the freeze-out cosmology the last term is negligible due to the long lifetime of N_2 . Moreover, m_{33} is aligned with the neutrino mass eigenstate m_3 [35]. In the freeze-in cosmology, we assume that the last term is less than 10^{-3} eV, since otherwise Y_B , (5.4), is strongly suppressed from strong washout effects.⁵ Unlike the freeze-out cosmology, m_{33} is not necessarily m_3 , but $\mathcal{O}(0 - 0.1 \text{ eV})$, since m_{23} may be non-negligible.

⁵If $y_{33}^2 v^2/M_2$ is taken much greater than $\mathcal{O}(0.1 \text{ eV})$, it is possible that y_{33}^2 commensurately grows to ensure m_{33} remains $\mathcal{O}(0.1 \text{ eV})$. Although this appears to enhance ϵ by increasing y_{33}^2 , the strong washout reduces Y_B by a slightly higher power, so the net effect is a decrease in Y_B . We avoid this route.

Avoiding a finely tuned cancellation between the two terms, y_{33} is maximized when the two terms are comparable, giving $y_{33} \sim m_{33}v_R/v^2$. This leads to a maximal natural value for the asymmetry parameter

$$\epsilon_* \equiv \frac{m_3^2 v_R^2}{8\pi v^4} \sim 10^{-11} \left(\frac{v_R}{10^{10} \text{ GeV}} \right)^2 \left(\frac{m_{33}}{0.05 \text{ eV}} \right)^2. \quad (5.11)$$

Using this value for ϵ , the baryon asymmetry in the freeze-out plus dilution cosmology (5.2) is too small, except for the very highest values of $v_R \sim 3 \times 10^{12}$ GeV as shown by the dot-dashed contour labeled ϵ_* in Fig. 4. Hence, except for a very small region near $v_R \sim 3 \times 10^{12}$ GeV, simultaneous N_1 dark matter and N_2 leptogenesis requires an enhancement of ϵ above ϵ_* . By comparing (5.11) with the contours of required ϵ in Fig. 4, it is apparent that the enhancement must be very significant at lower values of v_R . A similar conclusion applies to leptogenesis with freeze-in dark matter, (5.4).

There are two possibilities for this enhancement. One is to take $y_{33} \gg m_{33}v_R/v^2$ by having $m_3^{(5)}, m_{33}^{(ss)} \gg |m_{33}|$ so that a cancellation between the two terms of (5.10) occurs. Alternatively, $g(x)$ may be large when M_2 and M_3 are nearly degenerate (i.e. $x \simeq 1$). It is useful to introduce

$$\chi \equiv \frac{m_3^{(5)} - m_{33}^{(ss)}}{m_3^{(5)} + m_{33}^{(ss)}} = \frac{m_{33}}{m_3^{(5)} + m_{33}^{(ss)}}. \quad (5.12)$$

As χ goes to zero, the fine-tuning between the dimension-five and see-saw masses increases since each becomes larger than m_{33} and hence increasingly degenerate so as to keep their difference equal to m_{33} . That is, as $\chi \rightarrow 0$, M_3 grows (so that $m_3^{(5)}$ increases) and y_{33}^2 grows (even faster than M_3 , so that $m_{33}^{(ss)}$ increases) in the following manner:

$$M_3 = m_{33} \frac{v_R^2}{v^2} \frac{1 + \chi}{2\chi} \quad (5.13)$$

$$y_{33}^2 = m_{33}^2 \frac{v_R^2}{v^4} \frac{(1 + \chi)(1 - \chi)}{4\chi^2}. \quad (5.14)$$

Note that $-1 < \chi < 1$ and that the sign of m_{33} is the same as the sign of χ . For the freeze-out cosmology, $m_{22} = m_2 = m_2^{(5)}$ is always positive. In terms of χ and ϵ_* of (5.11), the lepton asymmetry parameter can be written as

$$\epsilon = \epsilon_* \frac{(1 + \chi)(1 - \chi)}{4\chi^2} g(x) \sin^2 \alpha \sin 2\beta. \quad (5.15)$$

The observed baryon asymmetry can be explained by the enhancement from small χ and/or $x \simeq 1$.

We focus on the freeze-out cosmology for the rest of this subsection and identify m_{22} and m_{33} with m_2 and m_3 , respectively. Combining (5.2), (5.11), and (5.15), the baryon asymmetry produced by N_2 decays is

$$\frac{Y_B}{8 \times 10^{-11}} = 10^{-5} \frac{2 \text{ keV}}{M_1} \left(\frac{v_R}{10^{10} \text{ GeV}} \right)^2 \left(\frac{m_3}{0.05 \text{ eV}} \right)^2 \frac{(1 + \chi)(1 - \chi)}{4\chi^2} g(x) f_B \sin^2 \alpha \sin 2\beta. \quad (5.16)$$

Since m_2 is dominated by the dimension 5 contribution to its mass,

$$x = \frac{M_3^2}{M_2^2} = \frac{m_3^2 (1 + \chi)^2}{m_2^2 4\chi^2}. \quad (5.17)$$

This is an important result since it shows that x and χ are not independent; they are related by the neutrino spectrum. The two choices for enhancing ϵ , x near unity and small χ , are seen to be mutually exclusive: if $\chi \ll 0.1$ then $x \gg 1$ for any realistic neutrino spectrum. Thus N_1 freeze-out dark matter and leptogenesis from N_2 decay requires either x near unity or small χ .

For the case of x very close to unity, χ is fixed from (5.17), giving

$$\chi \simeq \left(\frac{-1}{1 + 2\sqrt{r}}, -\frac{1}{1 \pm 2/\sqrt{r}}; 1 - r, -\frac{1}{3}(1 \pm \frac{r}{3}) \right), \quad r = \frac{\Delta m_{\text{sol}}^2}{\Delta m_{\text{atm}}^2} \quad (5.18)$$

where the first two cases are for a normal hierarchy, with $|m_3| > m_2$ and $|m_3| < m_2$, respectively, while the last two cases are for the inverse hierarchy with m_3 positive (and $m_2 > m_3$), and negative. These give values for the enhancement factor of

$$\frac{(1 + \chi)(1 - \chi)}{4\chi^2} g(x) \simeq (0.20, 30; 0.015, 1.96) \frac{1}{1 - x}. \quad (5.19)$$

We see that the inverse hierarchy requires $g(x)$ to be larger than in the normal hierarchy. Using this result, for the normal hierarchy with $|m_3| < m_2$, we find the observed baryon asymmetry results for

$$x - 1 \simeq 2 \frac{|M_2 - M_3|}{M_{2,3}} \simeq 1 \times 10^{-5} \left(\frac{2 \text{ keV}}{M_1} \right) \left(\frac{v_R}{10^{10} \text{ GeV}} \right)^2 \left(\frac{m_3}{0.01 \text{ eV}} \right)^2 f B \sin^2 \alpha \sin 2\beta. \quad (5.20)$$

For the case of a cancellation of large contributions to the neutrino mass m_3 , with χ very small, we find that (5.17) gives $g(x) \sim 3\chi(m_2/m_3) \ll 1$, so that the observed baryon asymmetry requires

$$\chi \simeq 0.75 \times 10^{-5} \left(\frac{2 \text{ keV}}{M_1} \right) \left(\frac{v_R}{10^{10} \text{ GeV}} \right)^2 \left(\frac{m_3 m_2}{(0.05 \text{ eV})^2} \right) f B \sin^2 \alpha \sin 2\beta. \quad (5.21)$$

We conclude that N_1 DM from freeze-out and leptogenesis from N_2 decay can occur simultaneously throughout the large unshaded region of Fig. 4. Enhancements in ϵ are required and can arise in two ways: near degeneracy of $M_{2,3}$ or large y_{33} with m_3 resulting from a cancellation between seesaw and dimension 5 contributions. In the next section we study whether leptogenesis can be obtained naturally, considering both the origin in the enhancement for ϵ and the effects of radiative corrections from y_{33} on the N_1 lifetime.

5.3 Restriction on neutrino masses in freeze-in cosmology

In the freeze-in cosmology without leptogenesis, discussed in Sec. 4.2, y_{i2} is not necessarily small since N_2 need not be long-lived. Consequently, m_{22} may possess a substantial contribution from $m_{22}^{(ss)}$, spoiling the direct relationship between M_2 and v_R of Eq. (4.5) required

for the freeze-out cosmology. However, requiring efficient leptogenesis in the freeze-in N_1 DM cosmology puts restrictions on the neutrino mass matrix.

To avoid the strong wash-out and maximize the allowed parameter space, the see-saw contribution from N_2 is required to be negligible. Then the SM neutrino masses are determined by the see-saw contribution from N_3 , $m_2^{(5)}$, and $m_3^{(5)}$.

The enhancement of the asymmetry requires $M_3 \gtrsim M_2$ for the following reasons. For enhancement by degeneracy, $M_3 = M_2$. For enhancement by tuning in m_{33} , if $M_2 > M_3$, $m_2^{(5)}$ must be also cancelled by $m_{22}^{(ss)}$ from N_3 , giving $y_{33}^2 \simeq M_3^2/v_R^2$ and $y_{23}^2 \simeq M_2 M_3/v_R^2$. However, $m_{23}^{(ss)} \simeq y_{23} y_{33} v^2/M_3 \simeq \sqrt{M_2 M_3} v^2/v_R^2$ becomes much larger than the observed SM neutrino masses.

Since $M_3 \gtrsim M_2$, the see-saw contribution from N_3 to m_{22} , $y_{23}^2 v^2/M_3$ is also negligible. We obtain a relation similar to Eq. (4.5),

$$M_2 \simeq m_{22} \left(\frac{v_R}{v} \right)^2. \quad (5.22)$$

Moreover, $m_2^{(5)}$ must be as large as the observed neutrino masses. Suppose that it is negligible. To obtain the two observed non-zero neutrino mass eigenvalues, m_{23} must be non-negligible. Since y_{23} is required to be small to avoid strong wash-out, y_{33} must compensate it. Then $m_{33}^{(ss)}$ is large, requiring the cancellation with $m_3^{(5)}$ and hence $y_{33}^2 \simeq M_3^2/v_R^2$. However,

$$m_{23}^{(ss)} \simeq \frac{y_{23} y_{33} v^2}{M_3} \simeq y_{23} \frac{v^2}{v_R^2} < \frac{(0.001 \text{eV})^{1/2} M_2^{1/2} v}{v_R} < (0.001 \text{eV})^{1/2} (0.1 \text{eV})^{1/2} = 0.01 \text{eV}, \quad (5.23)$$

which is not large enough to explain the SM neutrino masses. We conclude that m_{22} in Eq. (5.22) must be 0.01 – 0.05 eV.

6 Naturalness and radiative corrections in the effective field theory

For N_1 to be dark matter, whether in the context of (SM+N) or of Left-Right symmetry, small parameters must be introduced to limit its mass and decay rate, $M_1/M_{2,3}$, $y_{i1} \ll 1$. For sufficient cosmological stability, (3.6) can be approximated by

$$y_{i1} \lesssim 3 \times 10^{-13} \left(\frac{3 \text{keV}}{M_1} \right)^{3/2}. \quad (6.1)$$

The value of $M_1/M_{2,3}$ is model-dependent. In LR Higgs Parity, taking the examples of (4.5) or (5.14) with $|\chi|$ not tuned to be small,

$$\frac{M_1}{M_{2,3}} \simeq (10^{-12} - 10^{-13}) \left(\frac{M_1}{3 \text{keV}} \right) \left(\frac{10^{11} \text{GeV}}{v_R} \right)^2. \quad (6.2)$$

Quite generally, light sterile neutrino dark matter has a small numbers problem.

In (SM+N), with the N interactions of (1.2), the smallness of y_{i1} and M_1 can result from an approximate global symmetry under which only N_1 transforms. However, since freeze-in production of N_1 via y_{i1} violates (6.1), the only available production mechanism is via neutrino oscillations, and this also violates (6.1) unless it is enhanced by a very high lepton asymmetry [75].

In LR symmetric theories, N_1 may be produced by the $SU(2)_R \times U(1)_{B-L}$ gauge interactions. However, the smallness of the coupling y_{i1} seems to be hard to understand. We need a hierarchy $y_{i1} \ll y_{jk}^e$, despite the right-handed neutrinos and the right-handed charged leptons coming from the same $SU(2)_R$ doublets $\bar{\ell}$. A similar problem arises from the hierarchies $y_{i1} \ll y_{i2}, y_{i3}$ and $M_1 \ll M_{2,3}$. The observed large neutrino mixing angles imply no large symmetry distinction between the ℓ_i , and the LR symmetry then implies there are none between the $\bar{\ell}_i$. Then no symmetry can distinguish y_{i1} from y_{i2}, y_{i3} , nor M_1 from $M_{2,3}$.

While one can simply choose y_{i1} and M_1 to be small, in this and the next section we seek an explanation for their suppression. At the tree-level, it is possible to obtain the desired hierarchies of parameters by breaking $U(3)_q \times U(3)_{\bar{q}} \times U(3)_\ell \times U(3)_{\bar{\ell}} \times U(1)_{H_L} \times U(1)_{H_R}$ by appropriate symmetry breaking fields. However, because of the absence of symmetry protection mentioned above, quantum corrections may destabilize the hierarchies.

To make a comparison, we first examine the conventional LR symmetric theory with an $SU(2)_L \times SU(2)_R$ bi-fundamental and point out the difficulty in guaranteeing the stability of N_1 . We then argue why the problem can be avoided in Left-Right Higgs Parity, deferring the presentation of a UV completion to the next section. We show that the lepton sector of (2.4) and (2.5) has a naturalness problem if the cut-off scale of those interactions are far above v_R : in certain regions of parameter space, radiative contributions to y_{i1} and M_1 violate (6.1) and (6.2). This gives significant naturalness constraints on N_1 dark matter and on leptogenesis from N_2 decay. The UV completion discussed in the next section will also solve this problem.

6.1 Conventional LR symmetric theories

In the conventional LR symmetric theories, the SM Higgs is embedded into an $SU(2)_L \times SU(2)_R$ bi-fundamental scalar Φ , which can be decomposed under $SU(2)_L \times U(1)_Y$ as

$$\Phi = (H_u, H_d), \quad H_u : (2, \frac{1}{2}), \quad H_d : (2, -\frac{1}{2}). \quad (6.3)$$

In order for N_1 to be stable, the SM Higgs must almost exclusively come from only one of H_u or H_d . In fact, the charged lepton Yukawa coupling arises from

$$\mathcal{L} = y_{ij}^e \ell_i \Phi \bar{\ell}_j = y_{ij}^e \ell_i H_d \bar{e}_j + y_{ij}^e \ell_i H_u N_j \quad (6.4)$$

with the SM Higgs H containing H_d . In the basis where the N_i mass matrix is diagonal, y_{i1}^e is as large as $y_\tau \sim 10^{-2}$. To satisfy (6.1), the fraction of H_u in the SM Higgs must be very small. This can be achieved by coupling $\Phi\Phi^\dagger$ to an $SU(2)_R$ triplet that spontaneously breaks $SU(2)_R$, thereby splitting the masses of H_u and H_d . Also, the operators Φ^2 and $\ell\Phi^\dagger\bar{\ell}$ must be suppressed, since the former introduces $H_u - H_d$ mixing and the latter introduces

the Yukawa coupling of N to ℓH_d^\dagger . This can be achieved by a non-zero charge of Φ under some symmetry.

We must also introduce up and down quark Yukawa couplings,

$$\mathcal{L} = y^u q \Phi^\dagger \bar{q} + y^d q \Phi \bar{q}. \quad (6.5)$$

These terms necessarily break the aforementioned symmetry of Φ . The dominant effect comes from the quantum correction to the mass of Φ from the quark loop,

$$\Delta \mathcal{L} \sim \frac{y^{t*} y^b}{16\pi^2} \Lambda^2 \Phi^2 + \text{h.c.} \sim 10^{-4} \Lambda^2 \Phi^2 + \text{h.c.}, \quad (6.6)$$

where Λ is the cut-off of the theory. This introduces $H_u - H_d$ mixing and the Yukawa coupling of N ,

$$\mathcal{L} = y_{ij} \ell_i H N_j, \quad y_{ij} \sim 10^{-4} \frac{\Lambda^2}{m_{H_u}^2} y_{ij}^e \sim 10^{-6} \frac{\Lambda^2}{m_{H_d}^2} > 10^{-6}, \quad (6.7)$$

violating the bound (6.1).

This problem can be avoided by using different Φ s for quark and lepton Yukawa couplings and/or introducing supersymmetry, but we do not pursue this direction further.

6.2 Left-right Higgs Parity

The coupling y_{ij} receives quantum correction also in Left-Right Higgs Parity. The quantum correction from the quark and charged lepton Yukawa couplings is given by the Feynman diagram in Fig. 5. We estimate this radiative correction to y_{i1} to be

$$\Delta y_{i1} \sim \frac{1}{(16\pi^2)^2} 3y_t y_b y_\tau U_{\tau I_i} U_{\tau I_1}^* \left(\frac{\Lambda_c}{v_R} \right)^2 \simeq 10^{-9} \left(\frac{\Lambda_c}{v_R} \right)^2, \quad (6.8)$$

where the PMNS matrix U appears in the charged current $\bar{e} U \gamma^\mu \nu$, and I_i is the standard PDG numbering for the LR partner of N_i . In the following we take $U_{\tau I} \sim 0.5$. This correction is quadratically divergent, for loop momenta above v_R up to Λ_c , the cutoff of the effective theory with the dimension-five operators for the charged fermion masses of (2.4). The stability of N_1 , (3.6), requires $y_{i1} \lesssim 10^{-13}$ for any M_1 , which is violated for $\Lambda_c > v_R$. The dimension-five operators may be, however, UV-completed by introduction of particles with masses below v_R . In the next section, we present such a setup and show that the quantum correction to y_{i1} can be suppressed.

Successful leptogenesis from N_2 decay requires y_{33} to be sufficiently large. Since the flavor symmetry that distinguishes N_1 from $N_{2,3}$ is broken by the charged lepton Yukawa couplings, quantum corrections involving y_{33} and the charged lepton Yukawas generate non-zero y_{i1} . Similarly, M_1 should also receive quantum corrections from $M_{2,3}$ and charged lepton Yukawa couplings.

The Feynman diagrams for quantum corrections to y_{i1} and M_{1j} from the lepton sector are shown in Fig. 6. Two further diagrams involve the same vertices with different connections

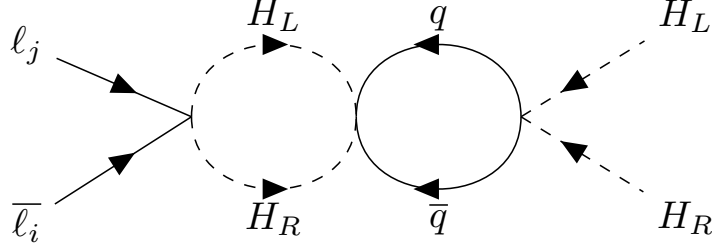


Figure 5. Radiative corrections to y_{i1} from charged leptons and quarks in the EFT. Loop momenta near the quark EFT cutoff scale, Λ_c , lead to (6.8).

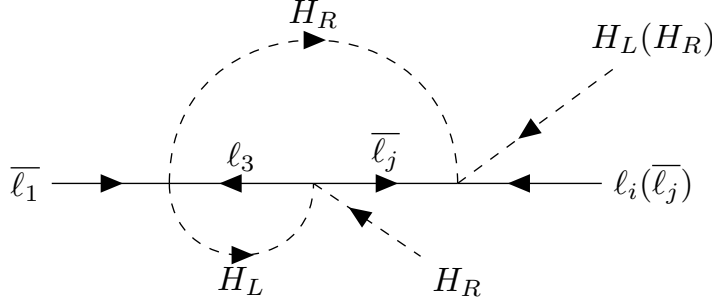


Figure 6. Radiative corrections to y_{i1} and M_{1j} (parenthesis) in the EFT. Loop momenta near the EFT cutoff scale lead to (6.9) and (6.11).

of the Higgs lines. They are quadratically divergent for loop momenta above v_R up to Λ , the cutoff of the effective field theory described by the Lagrangian (2.5) and the third term of (2.4). We estimate this radiative correction to y_{i1} to be

$$\Delta y_{i1} \sim \frac{1}{(16\pi^2)^2} \sum_{j=2,3} y_{ij} y_\tau^2 U_{\tau I_j} U_{\tau I_1}^* \left(\frac{\Lambda}{v_R} \right)^2. \quad (6.9)$$

Requiring this radiative correction to y_{i1} not exceed the limit of (6.1) from the radiative decay of N_1 bounds y_{ij} ($i, j = 2, 3$),

$$y_{ij} \lesssim y_{\max} = \frac{M_1 \sin 2\theta_{1\text{exp}}}{v} \frac{(16\pi^2)^2}{0.25 y_\tau^2} \left(\frac{v_R}{\Lambda} \right)^2 \lesssim 10^{-5} \left(\frac{3 \text{ keV}}{M_1} \right)^{3/2} \left(\frac{10}{\Lambda/v_R} \right)^2, \quad (6.10)$$

where we used $U_{\tau I_1}^* U_{\tau I_j} \sim 0.25$ and assumed no cancellation in (6.9) between $j = 2$ and $j = 3$ contributions. For N_1 dark matter, whether by freeze-out or freeze-in, y_{ij} may be chosen small enough to satisfy this bound. However, leptogenesis requires a significant y_{33} and we discuss this below.

Similarly, diagrams such as the one in Fig. 6 lead to radiative corrections to the $\bar{\ell}_1 \bar{\ell}_j H_R H_R$ operator

$$\Delta M_{j1} \sim \frac{1}{(16\pi^2)^2} M_j y_\tau^2 U_{\tau I_j} U_{\tau I_1}^* \left(\frac{\Lambda}{v_R} \right)^2. \quad (6.11)$$

Diagonalizing the N mass matrix leads to a radiative correction to M_1 from $M_{2,3}$

$$\Delta M_1 \sim \frac{1}{(16\pi^2)^4} M_{2,3} (0.25 y_\tau^2)^2 \left(\frac{\Lambda}{v_R}\right)^4. \quad (6.12)$$

For this not to exceed the value of $M_1/M_{2,3}$ given in (6.2) requires

$$M_1 \gtrsim 3 \text{ keV} \left(\frac{v_R}{10^{12} \text{ GeV}}\right)^2 \left(\frac{\Lambda/v_R}{10}\right)^4, \quad (6.13)$$

where we assumed no cancellation between $j = 2, 3$ contributions. Thus, for N_1 dark matter, a cutoff $\Lambda = 10 v_R$ just allows the entire triangular regions of Fig. 2 for the freeze-out cosmology but limits very large v_R in Fig. 3 for the freeze-in cosmology.

The quadratically divergent correction to y_{i1} (6.9) places a naturalness constraint on y_{33} and therefore, via (5.8), on leptogenesis

$$\epsilon \lesssim 3 \times 10^{-12} \left(\frac{3 \text{ keV}}{M_1}\right)^3 \left(\frac{10}{\Lambda/v_R}\right)^4 g(x) \sin^2 \alpha \sin 2\beta. \quad (6.14)$$

This is far below the required values of ϵ shown in Fig. 4 for freeze-out dark matter and given in (5.4) for freeze-in cosmology, unless $g(x) \gg 1$.⁶ This requires x near unity and, from (5.14) and (5.17), $y_{33} \sim m_3 v_R/v^2$. Requiring this value of y_{33} to satisfy the bound of (6.10) leads to the naturalness constraint

$$\left(\frac{M_1}{3 \text{ keV}}\right)^{3/2} \left(\frac{v_R}{10^{10} \text{ GeV}}\right) \lesssim \left(\frac{10}{\Lambda/v_R}\right)^2 \quad (6.15)$$

shown by blue lines in Fig. 7. Thus, in the EFT the quadratic divergence of y_{i1} greatly limits the range of (M_1, v_R) that naturally allows successful leptogenesis.

In the next section we give a UV completion of the lepton and quark sector. This is important for two reasons: first it provides an understanding for why N_1 is very light and long-lived, and second it allows a very large reduction in the radiative corrections for y_{i1} and M_1 , reopening large regions of the (M_1, v_R) plane to natural leptogenesis.

7 A UV Completion yielding a light, long-lived N_1

As we have seen in the previous section, to naturally protect the stability of N_1 against quantum corrections, the UV completion of the dimension-5 operators (2.4) and (2.5) should occur at a mass scale below v_R for the correction from Fig. 5, and at the most, not far above v_R for the correction from Fig. 6. In this section, we present a UV completion and show that the quantum corrections can be sufficiently suppressed.

⁶We will discuss a natural origin for $g(x) \gg 1$ in Sec. 8.

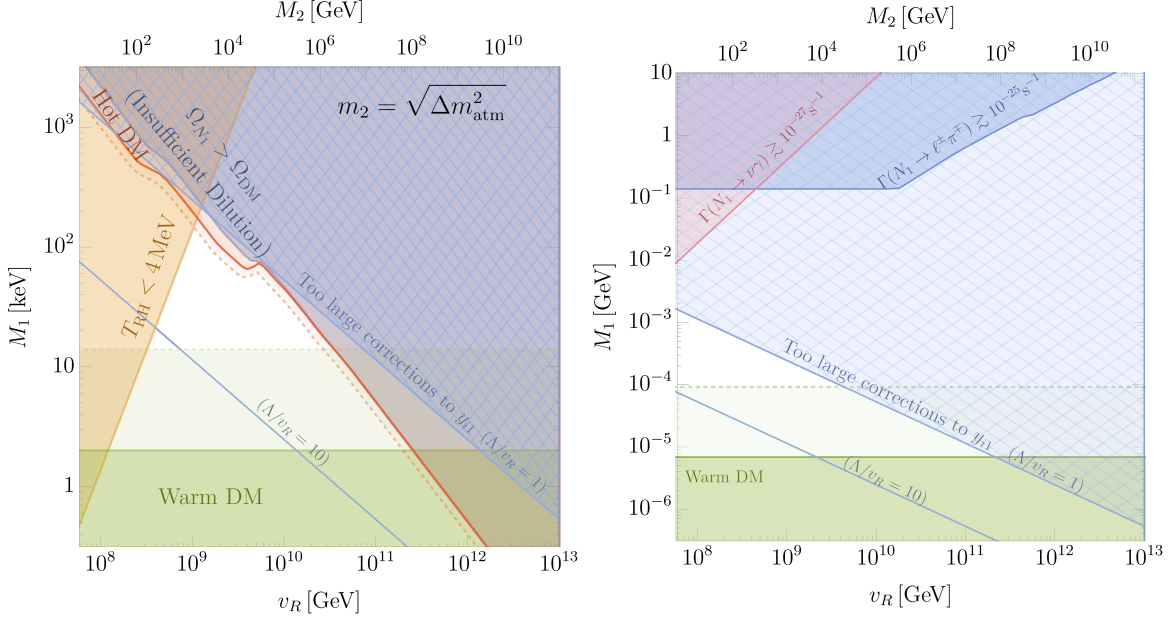


Figure 7. The parameter space where the mass and stability of N_1 DM can be realized without fine tuning in the effective theory $\ell\ell H_L H_L + \bar{\ell}\bar{\ell} H_R H_R + \ell\bar{\ell} H_L H_R$. The charged fermion masses are UV completed below v_R to avoid the radiative correction of Fig. 5. In the hatched blue region, the value of y_{33} required to set $x \equiv (M_3/M_2)^2 \simeq 1$ for leptogenesis, approximately $m_{33}v_R/v^2$, is sufficiently large that the tree and loop contributions to y_{i1} must be unnaturally tuned to keep N_1 stable when $\Lambda/v_R = 1$. Λ is the UV cutoff. The lower blue contour shows the same region if $\Lambda/v_R = 10$. The unhatched shaded regions are constraints solely on N_1 DM in the freeze-out (left) and freeze-in (right) cosmologies, as in Figs. 2 and 3.

7.1 The UV completion: tree-level

The operators $\ell\ell H_L H_L$, $\bar{\ell}\bar{\ell} H_R H_R$ and $\ell\bar{\ell} H_L H_R$ can be obtained by introducing singlet fields S_a and \bar{S}_a with the following couplings and masses,

$$\mathcal{L} = \lambda_{ia} \bar{\ell}_i \bar{S}_a H_L + \bar{\lambda}_{ia} \bar{\ell}_i S_a H_R + \frac{1}{2} M_{\bar{S},a} \bar{S}_a \bar{S}_a + \frac{1}{2} M_{S,a} S_a S_a + M_{S\bar{S},ab} S_a \bar{S}_b + \text{h.c.},$$

$$\bar{\lambda}_{ia} = \lambda_{ia}^*, \quad M_{\bar{S},a} = M_{S,a}, \quad M_{S\bar{S},ab}^* = M_{S\bar{S},ba}, \quad (7.1)$$

and integrating out S and \bar{S} . With three pairs of S and \bar{S} , the neutrino sector has $U(3)_\ell \times U(3)_{\bar{\ell}} \times U(3)_S \times U(3)_{\bar{S}} \times U(1)_{H_L} \times U(1)_{H_R}$ flavor symmetry. Hierarchical breaking of the symmetry can explain the hierarchy $y_{i1} \ll y_{i2}, y_{i3}$ and $M_1 \ll M_{2,3}$. We assume flavor symmetry breaking such that among three pairs of S and \bar{S} , only two pairs have significant coupling λ and/or small masses M_S ; we may instead start from the theory where only two pairs of S and \bar{S} are present. This suppresses the quantum correction to y_{i1} and M_1 for the following reason. Although the vertex corrections to λ from the tau Yukawa may couple $\bar{\ell}_1$ to S , one linear combination of $\bar{\ell}_i$ does not couple to \bar{S} . We may redefine the linear combination as $\bar{\ell}_1$, which is light. The operator $\ell\bar{\ell} H_L H_R$ is obtained from the mass term $M_{S\bar{S}} S\bar{S}$. This gives

rise to Yukawa couplings between the massive linear combinations of ℓ_i and of $\bar{\ell}_i$, but the massless combinations, which do not couple to S and \bar{S} , do not obtain Yukawa couplings.

If there are (effectively) only two pairs of S and \bar{S} , the $U(3)_\ell \times U(3)_{\bar{\ell}}$ symmetry may be anarchically broken in the neutrino sector. This model explains why N_1 is much lighter and has a smaller Yukawa coupling than $N_{2,3}$. However, to show that N_1 is sufficiently light and stable, we must study higher-dimensional operators from the cutoff scale of the theory M_{cut} , e.g. the Planck scale (and, in the next subsection, from radiative corrections). If the $U(3)_\ell \times U(3)_{\bar{\ell}}$ symmetry is anarchically broken, the following higher-dimensional operators are allowed:

$$\mathcal{L} \sim \frac{\bar{\lambda}^2 M_S^*}{M_{\text{cut}}^2} \bar{\ell} \ell H_R H_R + \frac{\lambda \bar{\lambda} M_{S\bar{S}}^*}{M_{\text{cut}}^2} \ell \bar{\ell} H_L H_R, \quad (7.2)$$

with λ and $\bar{\lambda}$ being typical entries in the matrices λ_{ia} and $\bar{\lambda}_{ia}$.⁷ These operators give N_1 a mass and a coupling to ℓH with values

$$\begin{aligned} \Delta M_1 &\simeq \frac{\lambda^2 M_S v_R^2}{M_{\text{cut}}^2} \simeq \left(\frac{M_S}{M_{\text{cut}}} \right)^2 M_3 \simeq \text{keV} \frac{M_3}{m_\nu (v_R/v)^2} \left(\frac{v_R}{3 \times 10^{11} \text{GeV}} \right)^4 \left(\frac{M_S}{v_R} \right)^2 \left(\frac{M_{\text{Pl}}}{M_{\text{cut}}} \right)^2, \\ \Delta y_{i1} &\simeq \frac{\lambda^2 M_{S\bar{S}} v_R}{M_{\text{cut}}^2} \simeq \frac{M_S^2}{M_{\text{cut}}^2} y_{33}, \end{aligned} \quad (7.3)$$

where we take the largest M_i and y_{ij} , i.e. M_3 and y_{33} . It is possible to reduce the size of these corrections by taking M_S smaller than v_R , when $H_R = v_R$ in (7.1) and (7.2). In this case the effective theory below M_S takes the form of Eq. (2.5) with H_R replaced with v_R . It is clear that (7.3) can satisfy (6.1) and (6.2) for the range of v_R of interest.⁸ We delay a discussion of the implications of these results as the quantum corrections to y_{i1} are larger than the tree result of (7.3), unless $v_R > 10^{-4} M_{\text{cut}}$.

In the model without \bar{S} , shown in Eq. (8.3), $M_{S\bar{S}}$ in Eq. (7.2) is replaced by M_S , but the corrections to M_1 and y_{i1} are still given by Eq. (7.3).

7.2 The UV completion: quantum corrections

7.2.1 Corrections from lepton Yukawas

We first discuss the quantum corrections from y_{i2} , y_{i3} and charged lepton Yukawa couplings. All three $\bar{\ell}_i$ have Yukawa interactions in Eq. (2.4), among which the tau Yukawa is the largest. The tau Yukawa necessarily breaks the approximate or accidental symmetry of (7.1) that discriminates $\bar{\ell}_1$ from $\bar{\ell}_{2,3}$, and gives quantum contributions to M_1 and y_{i1} .

The quantum corrections depend on the UV model that generates the dimension-5 interactions in Eq. (2.4). Let us first consider the case where the charged lepton Yukawas arise

⁷Although M_S is a real parameter, we put the superscript $*$ to clarify the charge structure.

⁸In fact, further suppression results if supersymmetry exists in the UV, since holomorphy of the superpotential can forbid the operators in Eq. (7.2).

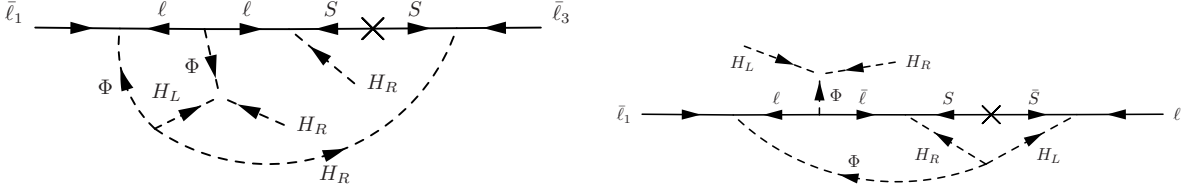


Figure 8. Two-loop diagrams correcting the mass and decay rate of the dark matter, N_1 , when the neutrino masses are generated by the exchange of a heavy singlet S , and the charged lepton masses are generated by the exchange of a heavy scalar, Φ . The diagrams are UV completions to the EFT diagrams of Fig. 6.

from the exchange of a heavy scalar Φ with charge $(1, 2, 2, 0)$,⁹

$$\mathcal{L} = -m_\Phi^2 |\Phi|^2 + (x_{ij} \Phi \ell_i \bar{\ell}_j - A \Phi^\dagger H_L^\dagger H_R^\dagger + \text{h.c.}). \quad (7.4)$$

After integrating out Φ and inserting the vev of H_R , we obtain the Yukawa coupling

$$y_{ij}^e = \frac{A v_R}{m_\Phi^2} x_{ij}. \quad (7.5)$$

The quantum correction above the scale M_S renormalizes λ and M_S but, by the approximate (accidental) symmetry, one linear combination of the N_i still has a small (zero) mass and coupling to ℓH_L . Only corrections below the scale M_S can change the mass and decay rate of N_1 . The two-loop diagram shown in the left panel of Fig. 8 dominantly corrects M_1 , generating

$$\begin{aligned} \mathcal{L} &\simeq \frac{1}{(16\pi^2)^2} \frac{M_{S,b} A^2}{m_\Phi^4} x_{1a} x_{3a}^* \lambda_{3b}^* \lambda_{3b}^* \bar{\ell}_1 \bar{\ell}_i H_R H_R \\ &\simeq \frac{0.25 y_\tau^2}{(16\pi^2)^2} M_3 \frac{M_S^2}{v_R^4} \bar{\ell}_1 \bar{\ell}_i H_R H_R, \end{aligned} \quad (7.6)$$

where we assume $M_S \ll m_\Phi$. In the second equality we use $x_{1a} x_{3a}^* A^2 / m_\Phi^4 = (U_{\tau I_1} U_{\tau I_i} y_\tau) (U_{\tau I_3} U_{\tau I_i} y_\tau)^* / v_R^2 \simeq (0.25 y_\tau^2 / v_R^2)$, and $\lambda^2 / M_S \simeq M_3 / v_R^2$. This term, after H_R obtains a vev, gives a mass mixing between N_1 and N_3 resulting in a correction to the mass of N_1

$$\Delta M_1 \simeq \left(\frac{0.25 y_\tau^2}{(16\pi^2)^2} \right)^2 \left(\frac{M_S}{v_R} \right)^4 M_3. \quad (7.7)$$

The mass mixing also induces a coupling of N_1 to ℓH ,

$$\Delta y_{i1} \simeq \left(\frac{0.25 y_\tau^2}{(16\pi^2)^2} \right) \left(\frac{M_S}{v_R} \right)^2 y_{i3}. \quad (7.8)$$

The diagram in the right panel of Fig. 8 also corrects y_{i1} by a similar amount.

⁹ Φ couples exclusively to leptons, not quarks, so that potential CP violating phases of Φ do not enter into the quark sector. Consequently, the strong CP problem remains solved when introducing Φ .

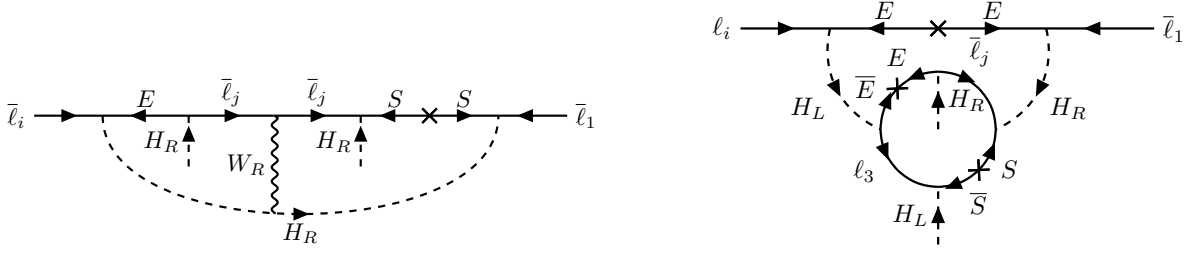


Figure 9. Two-loop diagrams correcting the decay rate and mass of the dark matter, N_1 , when the neutrino masses are generated by the exchange of a heavy singlet S , and when the charged lepton masses are generated by the exchange of a heavy fermion, E . The diagrams are UV completions to the EFT diagrams of Fig. 6.

We next consider the case where the charged lepton yukawas arise from the exchange of heavy fermions E and \bar{E} ,

$$\mathcal{L} = z_{ia}^e \ell_i \bar{E}_a H_L^\dagger + (z_{ia}^e)^* \bar{\ell}_i E_a H_R^\dagger + M_{E,a} E_a \bar{E}_a. \quad (7.9)$$

When $m_E > z^e v_R$, after integrating out E and inserting the vev of H_R , we obtain the yukawa coupling

$$y_{ij}^e = z_{ia}^e \frac{v_R}{M_{Ea}} z_{aj}^{e\dagger} \quad (7.10)$$

When $m_E < z^e v_R$, the SM right-handed charged leptons originate from \bar{E} , and the Yukawa coupling is $y^e \simeq z^e$. The two-loop diagram with external H_R and $\bar{\ell}_3$ in the left panel of Fig. 9 generates a mass-mixing between N_3 and N_1 ,¹⁰

$$\mathcal{L} \simeq \frac{1}{(16\pi^2)^2} g^2 z_{1a} z_{3a}^* \lambda_{3b}^* \lambda_{3b}^* \frac{M_{S,b}}{\text{Max} \{M_{E,a}^2, m_{H_R}^2\}} \bar{\ell}_1 \bar{\ell}_3 H_R H_R \quad (7.11)$$

$$\simeq \frac{1}{(16\pi^2)^2} \frac{M_S^2}{v_R^4} M_3 \bar{\ell}_1 \bar{\ell}_3 H_R H_R \times \begin{cases} (0.5y_\tau)^2 (z_{1a} z_{3a}^*)^{-1} & m_E \gtrsim v_R \\ (z_{1a} z_{3a}^*) & m_E \lesssim v_R. \end{cases} \quad (7.12)$$

In the second line, we use $z_{1a} z_{3a}^* = U_{\tau I_1} U_{\tau I_3} y_\tau M_{Ea} / v_R \simeq 0.25 y_\tau M_{Ea} / v_R$, and $\lambda^2 / M_S \simeq M_3 / v_R^2$. This term, after H_R obtains a vev, gives a mass mixing between N_1 and N_3 . For $m_E \gtrsim v_R$, the correction is minimized for the largest $z = O(1)$. For $m_E \lesssim v_R$, the correction is minimized for the smallest $z \approx y_\tau$. The smallest quantum correction is then

$$\Delta M_1 \gtrsim \left(\frac{0.25 y_\tau^2}{(16\pi^2)^2} \right)^2 \left(\frac{M_S}{v_R} \right)^4 M_3. \quad (7.13)$$

Similarly, the mass mixing also induces a coupling of N_1 to ℓH ,

$$\Delta y_{i1} \gtrsim \left(\frac{0.25 y_\tau^2}{(16\pi^2)^2} \right) \left(\frac{M_S}{v_R} \right)^2 y_{i3}. \quad (7.14)$$

¹⁰Without W_R in the diagram, one of external H_R must be charged.

The two-loop diagram in the right panel of Fig. 9 with external H_L and ℓ_i also corrects y_{i1} by a similar amount. We see that Eqs. (7.7) and (7.8), from a UV completion with Φ , or Eqs. (7.13) and (7.14), from a UV completion with E , are identical in form to Eqs. (6.12) and (6.9) with Λ replaced by M_S . Thus, with $M_S \ll v_R$ the naturalness of the theory is greatly improved. When we take $\Lambda/v_R < 1$, Λ should be interpreted as M_S .

7.2.2 Corrections from charged fermion Yukawa couplings

We next consider the quantum corrections from charged fermion Yukawa couplings. We introduce a UV completion for the up and down quark Yukawas by heavy fermions U, \bar{U} , and D, \bar{D} , with Lagrangian

$$\begin{aligned}\mathcal{L}_u &= z_{ia}^u q_i \bar{U}_a H_L + (z_{ia}^u)^* \bar{q}_i U_a H_R + M_{U,a} U_a \bar{U}_a, \\ \mathcal{L}_d &= z_{ia}^d q_i \bar{D}_a H_L^\dagger + (z_{ia}^d)^* \bar{q}_i D_a H_R^\dagger + M_{D,a} D_a \bar{D}_a.\end{aligned}\quad (7.15)$$

With $M_U > z^u v_R$, integrating out U generates the up quark Yukawa couplings

$$y_{ij}^u = z_{ia}^u \frac{v_R}{M_{U,a}} z_{aj}^{u\dagger} \quad (7.16)$$

via a seesaw, and similarly for the down quark Yukawas by integrating out D . When $m_U < z^u v_R$, on the other hand, the SM right-handed up quarks dominantly come from \bar{U} rather than \bar{q} , so that the light fermion masses are “flipped” rather than “seesaw”, with the Yukawa coupling $y^u \sim z^u$. In the up, down or charged lepton sectors, if $M > y v_R$ the light mass is seesawed, while it becomes flipped as M drops below $y v_R$.

When the heavy fermion masses M_U, M_D , are less than v_R , the cutoff scale of the EFT generating the dimension-five quark masses is below v_R . As a result, the quadratically divergent radiative corrections to y_{i1} as calculated in Eq. (6.8) and visualized in Fig. 5, are absent. The radiative corrections to y_{i1} in the UV complete theory are shown by the diagrams in Fig. 10, which generate the operator

$$\begin{aligned}\mathcal{L} \simeq \frac{1}{(16\pi^2)^2} \frac{M_U M_D}{v_R m_{H_R}^2} (z_{kb}^u z_{kb}^{u*}) (z_{lc}^d z_{lc}^{d*}) \ell_i \bar{\ell}_1 H_L H_R \times \begin{cases} \frac{M_E v_R}{M_*^2} (z_{ia}^e z_{1a}^{e*}) & : E \text{ exchange} \\ y_{i1}^e & : \Phi \text{ exchange} \end{cases}, \\ M_* = \max(M_U, M_D, M_E, z^u v_R, z^d v_R, z^e v_R),\end{aligned}\quad (7.17)$$

where we assume $M_{U,D,E} < m_{H_R}$. We consider the correction from the third generation fermions and their LR partners, since the smallest possible corrections are largest for the third generation. For $M_{U,D,E} > z^{u,d,e} v_R$, where we may integrate out the heavy fermions to obtain the dimension-5 operators, the quantum correction is bounded by

$$\Delta y_{i1} \gtrsim \frac{1}{(16\pi^2)^2} y_i^3 y_b^3 \times \begin{cases} y_\tau^3 & : E \text{ exchange} \\ y_\tau & : \Phi \text{ exchange.} \end{cases} \simeq \begin{cases} 10^{-18} & : E \text{ exchange} \\ 10^{-14} & : \Phi \text{ exchange.} \end{cases}, \quad (7.18)$$

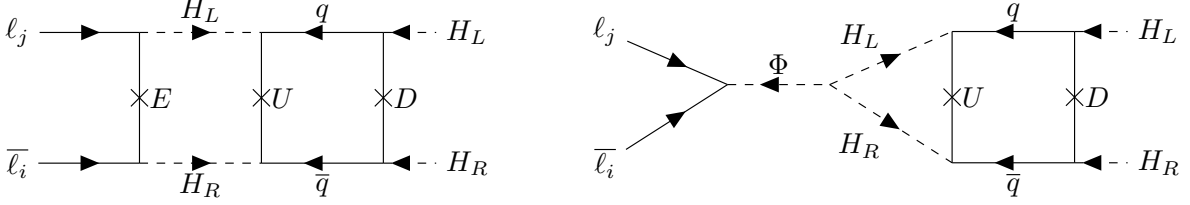


Figure 10. Two-loop diagrams correcting the decay rate of the dark matter, N_1 , when the charged lepton masses are generated by the exchange of a heavy fermion, E (left), or scalar, Φ (right), and the up-type quark and down-type quark masses are generated by the exchange of heavy fermions, U , D , respectively. Each diagram is a UV completion to the EFT diagram of Fig. 5.

where we take $M_* \sim v_R$. The correction is small enough for $M_1 < 10$ MeV/10 keV for E/Φ exchange. For $M_{U,D,E} < z^{u,d,e}v_R$, where the SM right-handed fermions are dominantly $\bar{U}, \bar{D}, \bar{E}$, the quantum correction is bounded by

$$\Delta y_{i1} \gtrsim \frac{1}{(16\pi^2)^2} y_t^3 y_b^3 \frac{M_U M_D}{y_t y_b v_R^2} \times \begin{cases} y_\tau^3 \frac{M_E}{y_\tau v_R} \\ y_\tau \end{cases}, \quad (7.19)$$

which is even smaller than (7.18).

In summary, these UV completions easily allow small M_1 to be natural throughout the allowed regions of Figs. 2 or 3 for any v_R consistent with Higgs Parity, $10^9 \text{GeV} \lesssim v_R \lesssim 10^{13} \text{GeV}$. The radiative correction of (7.7), from the left panel of Fig. 9, easily satisfies (6.2) for $M_S < v_R$. A possible tree-level contribution from the Planck scale, (7.3), is natural if $M_S/v_R \lesssim (M_1/\text{keV})^{1/2} (3 \times 10^{11} \text{GeV}/v_R)^2$.

Furthermore, corrections to the N_1 decay rate from Fig. 8 or 9 (Fig. 10) involving lepton (charged fermion) yukawa couplings, can be made small enough in either cosmology by choosing M_S (M_U, M_D, M_E) sufficiently less than v_R . For (7.8) or (7.14), the N_1 stability requirement (6.1) is satisfied if $M_S/v_R < (30 \text{keV}/M_1)^{3/4}$, where we took $y_{33} = 10^{-6}$, typical for natural leptogenesis. For radiative corrections involving “seesaw” charged fermions, (7.18) shows that the N_1 lifetime is natural for $M_1 < 10$ MeV/10 keV for E/Φ exchange; for “flipped” masses (7.19) shows that M_1 can naturally be much larger. Hence, the UV completion with the largest natural range for M_1 has charged lepton masses arising from E exchange, rather than Φ exchange, and has “flipped” rather than “seesaw” charged fermion masses. In such UV completions, the entire parameter of Figs. 2 or 3 can be made natural for N_1 DM.

For sufficiently small Dirac masses $M_{U,D,E} \ll z^{u,d,e}v_R$, the SM fermion masses are “flipped” with right-handed states dominantly $SU(2)_R$ singlets, \bar{U}, \bar{D} and \bar{E} . This may suppress the decay of N_2 by W_R exchange, relaxing the upper bound on v_R in the cosmology with freeze-out and dilution by N_2 . With “flipped” masses, \bar{q} and the charged component in $\bar{\ell}$ obtain large masses $z^{u,d,e}v_R = y^{u,d,e}v_R$. For v_R around the upper bound, N_2 can decay only

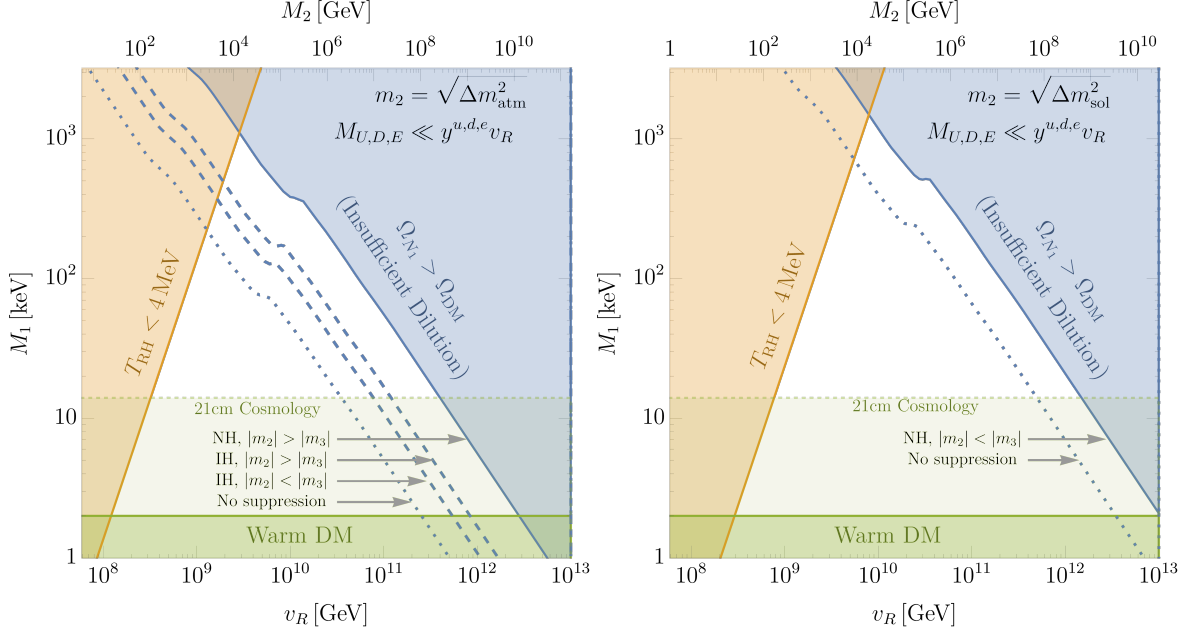


Figure 11. The parameter space of N_1 DM produced by relativistic freeze-out and dilution from N_2 decay when the masses of the heavy fermions, $M_{U,D,E}$, are far lighter than $y^{u,d,e}v_R$. The shaded regions are identical to Fig. 2, except that the beta decay rate of N_2 is suppressed, shifting the (blue) insufficient dilution region to higher v_R . The N_2 beta decay rate decreases as the two heaviest generations of \bar{q} and $\bar{\ell}$ becoming heavy, reducing the kinematically allowed decay channels and inducing suppressions from the PMNS matrix. We show the allowed regions for $m_2 = \sqrt{\Delta m_{\text{atm}}^2}$ (left) and $m_2 = \sqrt{\Delta m_{\text{sol}}^2}$ (right). The blue contours show how the insufficient dilution boundary depends on whether ν_2 and ν_3 obey a normal (NH) or inverted hierarchy (IH). Bounds from hot DM are discussed in the text.

into the first generation of \bar{q} and $\bar{\ell}$. The decay rate of N_2 via W_R exchange is

$$\Gamma_{N_2 \rightarrow (\ell^+ \bar{u} d, \ell^- u \bar{d})} + \Gamma_{N_2 \rightarrow N_1 \ell^+ \ell^-} = \frac{2}{1536\pi^3} \frac{M_2^5}{v_R^4} |U_{eI_2}|^2 (3 + |U_{eI_1}|^2). \quad (7.20)$$

The PMNS matrix elements are given by [76]

$$|U_{eI_2}|^2 = \begin{cases} |U_{e2}|^2 \simeq 0.30 & : \text{NH}, |m_2| < |m_3| \\ |U_{e3}|^2 \simeq 0.023 & : \text{NH}, |m_2| > |m_3| \\ |U_{e2}|^2 \simeq 0.30 & : \text{IH}, |m_2| > |m_3| \\ |U_{e1}|^2 \simeq 0.67 & : \text{IH}, |m_2| < |m_3| \end{cases},$$

$$|U_{eI_1}|^2 = \begin{cases} |U_{e1}|^2 \simeq 0.67 & : \text{NH} \\ |U_{e3}|^2 \simeq 0.023 & : \text{IH} \end{cases}. \quad (7.21)$$

The suppression is most significant for NH with $|m_2| > |m_3|$. If the active neutrinos obey an IH, the suppression is also strongest when $|m_2| > |m_3|$. The allowed parameter space of

N_1 DM is shown in Fig. 11 for all cases. The bounds from warmness and BBN are as in Fig. 2; but the suppression of the N_2 beta decay rate relaxes the blue bound that arises from insufficient dilution, permitting the highest allowed v_R to reach 10^{12-13} GeV. From (7.20), the fraction of N_1 DM that is hot is $|U_{eI_1}|^2/3 = 0.22(\text{NH}), 0.007(\text{IH})$. Thus, N_2 decaying dominantly via W_R exchange is excluded for NH and allowed for IH.

8 Natural leptogenesis

In this section we study the extent to which successful leptogenesis can occur without the need for fine-tuning of parameters. In Sections 3, 4 and 5 we simply chose parameters of our theory to obtain a realistic light neutrino spectrum, decay rates, masses and interactions for $N_{1,2}$ that satisfy the constraints required for dark matter, and parameters that enhance leptogenesis to realistic values. While this is certainly possible, in this section we study the extra naturalness constraints imposed on the (M_1, v_R) parameter space by requiring a natural theory without fine-tuning. We will use the UV completion described in the previous section that allows us to start with an understanding of why N_1 is light and sufficiently stable, and also limits the size of radiative corrections.

In Section 5 we have seen that sufficient leptogenesis typically requires an enhancement of ϵ that can occur by near degeneracy of N_2 and N_3 , or by increasing y_{33} so that a cancellation between contributions to the light neutrino masses is required. Can these parameter choices be made natural by introducing approximate symmetries in the UV completion? In addition, in the last section we found a radiative correction to y_{i1} proportional to y_{33} , leading to mixing between N_1 and ν_i . Can a sufficiently long lifetime for N_1 be naturally maintained in the presence of an enhanced y_{33} for leptogenesis?

8.1 Models for enhanced asymmetry parameter

Highly degenerate right-handed neutrinos, $M_2 \simeq M_3$, can be explained by introducing an approximate flavor symmetry ensuring that $c_{22} \simeq c_{33}$ and $c_{23} \simeq 0$ in Eq. (2.5). Such symmetries include an $SU(2)$ symmetry rotating (ℓ_2, ℓ_3) , or discrete symmetries $\ell_2 \leftrightarrow \ell_3$ and $\ell_2 \rightarrow -\ell_2$. The symmetry is explicitly broken in the coupling b_{ij} to explain the mass splitting of the two heaviest SM neutrinos.

The symmetry is also explicitly broken by the charged lepton Yukawa couplings. For example, when the charged lepton Yukawas arise from the exchange of a heavy scalar Φ of charge $(1, 2, 2, 0)$, as in (7.4), one-loop quantum corrections from the coupling $x\Phi\ell\bar{\ell}$ give a wave-function renormalization,

$$\begin{aligned} \mathcal{L} = & (1 + \delta Z_{22})N_2^\dagger \bar{\sigma} \partial N_2 + (1 + \delta Z_{33})N_3^\dagger \bar{\sigma} \partial N_3 + \left(\delta Z_{23}N_2^\dagger \bar{\sigma} \partial N_3 + \text{h.c.} \right), \\ \delta Z_{ij} \simeq & \frac{x_{ki}x_{kj}^*}{8\pi^2}, \end{aligned} \tag{8.1}$$

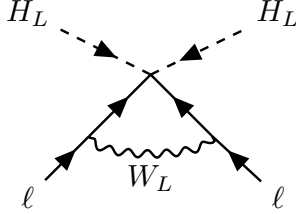


Figure 12. A diagram contributing to a non-zero neutrino mass for the case with tree-level cancellation between $m^{(5)}$ and $m^{(ss)}$.

where we conservatively do not include a log-enhancement. This generates a mass splitting

$$\frac{|M_2 - M_3|}{M_{2,3}} \simeq \sqrt{(\delta Z_{22} - \delta Z_{33})^2 + (\delta Z_{23} + \delta Z_{23}^*)^2} \gtrsim \frac{y_\tau^2}{8\pi^2} \simeq 10^{-6}, \quad (8.2)$$

where we use $|x_{ki}x_{kj}^*| \gtrsim y_\tau^2$. Near the resonance $x = 1$, $g(x) \simeq M_2/2(M_2 - M_3)$, so the maximum natural $g(x)$ is 5×10^5 . We obtain the same bound for the case when charged lepton masses are generated by heavy fermion exchange, as in (7.9). In summary, the maximum natural value for $g(x)$ is of order 10^6 .

Cancellation between the SM neutrino mass contributions from the see-saw of N_3 and the first dimension-5 operator of Eq. (5.10) can be explained in the following manner. Since we are interested in large y_{33} , we only consider ℓ_3 and $\bar{\ell}_3$, and drop generation indices. Let us introduce only one singlet S and couplings

$$\mathcal{L} = \lambda \ell S H_L + \lambda \bar{\ell} S H_R + \frac{1}{2} M_S S^2 + \text{h.c.} \quad (8.3)$$

Integrating out S gives the dimension-5 operator

$$\mathcal{L} = -\frac{\lambda^2}{2M_S} (\ell H_L + \bar{\ell} H_R)^2 + \text{h.c.}, \quad (8.4)$$

corresponding to Eq. (2.5) with $b_{33} = c_{33}$. Only one linear combination of ν and N , which is dominantly N , obtains a Majorana mass and hence the SM neutrino remains massless. This can be interpreted as a cancellation between $m^{(5)}$ and $m^{(ss)}$ in (5.12), giving $|\chi| \ll 1$.

Since there is no symmetry forbidding the Majorana mass of ν , it is generated by quantum corrections. Below the scale v_R , there is a quantum correction to $\ell \ell H_L H_L$ given by the diagram in Fig. 12, while there is no corresponding quantum correction to $\bar{\ell} \bar{\ell} H_R H_R$ and $\ell \bar{\ell} H_L H_R$. This quantum correction upsets the cancellation, giving a lower bound

$$|\chi| > \frac{g^2}{16\pi^2} \ln \left(\frac{\min(M_S, v_R)}{M_N} \right) \simeq 10^{-2}. \quad (8.5)$$

8.2 Radiative corrections: N_1 lifetime

Naturalness thus limits the maximum baryon asymmetry generated by N_2 in either cosmology,

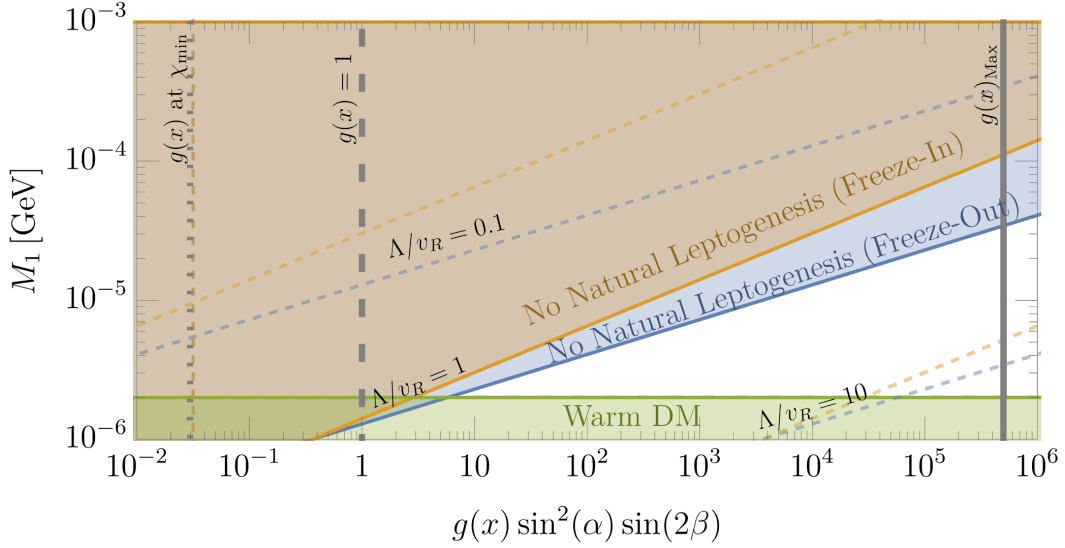


Figure 13. Parameter space for simultaneous N_1 DM and N_2 leptogenesis without fine-tuning. In the (blue, orange) shaded regions, the observed baryon asymmetry from N_2 decay, in the (freeze-out, freeze-in) cosmology, requires y_{33} so large that fine-tuning is needed for sufficient stability of N_1 , when $\Lambda = v_R$. The upper and lower dashed blue and orange contours show the analogous exclusion regions for $\Lambda/v_R = 0.1$ and $\Lambda/v_R = 10$, respectively. In the green shaded region, N_1 DM is too warm. In both freeze-out or freeze-in cosmologies, successful N_2 leptogenesis requires $g(x) > 1$ for $\Lambda \gtrsim v_R$; the greater Λ/v_R is, the more degenerate M_2 and M_3 must be to realize the observed baryon asymmetry. The vertical gray solid, dashed, and dotted lines show representative values of $g(x)$ when M_2 and M_3 have the maximal natural degeneracy ($g(x)_{\text{max}}$, solid), when M_2 and M_3 are comparable ($g(x) = 1$, dashed), and when $m_3^{(ss)}$ and $m_3^{(5)}$ are as naturally degenerate as can be ($g(x)$ at χ_{min} , dotted).

$$Y_B \lesssim \frac{28}{79} \frac{1}{8\pi} y_{\text{max}}^2 g(x) \sin^2 \alpha \sin 2\beta \begin{cases} \frac{\rho_{\text{DM}}/s}{M_1} & \text{(Freeze-Out + Dilution)} \\ \frac{\rho_{\text{DM}}/s}{M_1} + 0.03 \frac{m_2^{(ss)}}{10^{-4} \text{ eV}} Y_{\text{therm}} & \begin{pmatrix} \text{Freeze-In} \\ \text{Weak Washout} \end{pmatrix} \\ 0.03 Y_{\text{therm}} \left(\frac{m_2^{(ss)}}{10^{-2} \text{ eV}} \right)^{-1.16} & \begin{pmatrix} \text{Freeze-In} \\ \text{Strong Washout} \end{pmatrix} \end{cases}, \quad (8.6)$$

where y_{max} is given in Eq. (6.10).

The parameter space where Y_B is unable to reach the observed baryon asymmetry without tuning is shown in Fig. 13 in blue shading for the freeze-out cosmology and orange shading for the freeze-in cosmology, for $\Lambda/v_R = 1$. The dashed contours above and below show the analogous regions for $\Lambda/v_R = 0.1$ and $\Lambda/v_R = 10$, respectively. Because the radiative correction to the N_1 decay rate depends on the fourth power of Λ/v_R , the results are sensitive

to this ratio; natural leptogenesis becomes implausible for $\Lambda \gg v_R$. The allowed parameter space within the freeze-in cosmology is greater than the freeze-out cosmology due to the additional contribution to Y_B from $Y_{\ell H}$, which is assumed for the moment to saturate $0.1Y_{\text{therm}}$ for the purpose of showing the theoretical maximum allowed region of the freeze-in cosmology in Fig. 13. When $Y_{\ell H}$ is negligible compared to Y_{W_R} , the baryon asymmetry in the freeze-in cosmology is identical to the freeze-out cosmology and the orange region extends down to match the blue region.

The vertical gray lines show the asymmetry enhancement for three representative values of $g(x)$: when M_3 and M_2 are as naturally degenerate as can be ($g(x)_{\text{Max}}$, solid), when M_3 and M_2 are comparable ($g(x) = 1$, dashed), and when $m_3^{(ss)}$ and $m_3^{(5)}$ are as naturally degenerate as can be ($g(x)$ at χ_{min} , dotted).

A key result of Fig. 13 is that, for a theory with $\Lambda/v_R > 1$, natural leptogenesis requires $g(x) \gg 1$ in either cosmology, which is only possible when $x \equiv (M_3/M_2)^2$ is close to unity. Thus there are two ways to construct natural theories of leptogenesis. In the first, the structure of the theory below v_R is modified to remove the quadratic divergence of (6.9); such a theory is provided in Sec. 7. In the second, a symmetry is introduced to naturally yield near degeneracy of N_2 with N_3 , as discussed in Sec. 8.1.

The ratio (Λ/v_R) can be less than one if the effective field theory described by (2.4) and (2.5) is generated by physics below the scale v_R . In Sec 7 we construct an explicit model that generates (2.4) and (2.5) and show that in this theory the radiative corrections are given by (7.7) and (7.8), which are identical to (6.12) and (6.9) with Λ replaced by M_S , the mass of the fermion which upon integrating out generates the operators of (2.5). Thus, when we take $\Lambda < v_R$, we understand it to be the mass M_S of this fermion.

8.3 Natural leptogenesis for freeze-out cosmology

Although it appears the mass ratio M_3/M_2 can be freely adjusted to generate a large $g(x)$ independent of y_{33} , this is not the case as is shown in Section 5.2. This is because the neutrino mass matrix, (3.3), relates y_{33}, v_R, M_2 , and M_3 together in a way that ensures the active neutrino masses, m_2 and m_3 , remain $\mathcal{O}(0.1 \text{ eV})$. In the freeze-out cosmology, the smallness of y_{i1} and y_{i2} together with (3.3) require that m_2 and m_3 satisfy Eqs. (4.5) and (5.10), so that y_{33}^2 must not only be less than y_{max}^2 , but equal to

$$y_{33}^2 \simeq (\sqrt{x} m_2 - m_3) \sqrt{x} m_2 \frac{v_R^2}{v^4}. \quad \left(\begin{array}{l} \text{Constraint from neutrino masses} \\ \text{in freeze-out cosmology} \end{array} \right) \quad (8.7)$$

In Fig. 14, we show the constraints on (v_R, M_1) when incorporating leptogenesis naturally and consistently within the freeze-out N_1 DM cosmology. The shaded regions constraining N_1 DM remain from Fig. 2, but newly added is a hatched gold region where natural leptogenesis is inconsistent with the observed neutrino masses. Within the allowed region reside three triangles with the same representative values of M_3/M_2 (equivalently, $g(x)$), shown in Fig. 13: when M_3 and M_2 are as naturally degenerate as can be ($g(x)_{\text{max}}$, solid), when M_3 and M_2 are

comparable ($g(x) = 1$, dashed), and when $m_3^{(ss)}$ and $m_3^{(5)}$ are as naturally degenerate as can be ($g(x)$ at χ_{\min} , dotted), which occurs for $M_3 \gg M_2$. The right side of each triangle marks the region where y_{33} , as set by (8.7), is greater than y_{\max} , (6.10); that is, where neutrino masses are incompatible with a natural N_1 lifetime. The left side of the triangle, i.e. the boundary of the hatched gold region, marks the region where Y_B generated by N_2 (upper (8.6)), is unable to match the observed baryon asymmetry with y_{33} set by (8.7) and $\sin^2 \alpha \sin 2\beta = 1$; that is, where neutrino masses are incompatible with leptogenesis for the specified x . Within the unshaded region of each triangle, natural leptogenesis is possible for $\sin^2 \alpha \sin 2\beta < 1$. The gold, red, and green contours show the allowed regions when $\Lambda/v_R = 0.1, 1, \text{ and } 10$, respectively.

Among the four panels of Fig. 14, the variation in location of the naturally allowed region can be understood by the differences in the values and relative signs of m_2 and m_3 taken in each panel. This is because the apex of each triangle is determined by the value of y_{33}^2 that satisfies the neutrino mass relations, (8.7), and natural stability bounds for N_1 DM, (6.10). For the solid and dashed triangles, $x \approx 1$, and hence $y_{33}^2 \simeq m_2(m_2 - m_3)v_R^2/v^4$. When the active neutrinos obey an inverted hierarchy, as shown by the top two panels of Fig. 14, $m_2 \approx |m_3| \approx \sqrt{m_{\text{atm}}^2}$, so that if $m_3 < 0$, (top left panel), $m_2(m_2 - m_3) \simeq (0.1 \text{ eV})^2$, and if $m_3 > 0$, (top right panel), $m_2(m_2 - m_3) \ll (0.1 \text{ eV})^2$.¹¹ The first scenario gives a relatively larger value of y_{33}^2 compared to the second, meaning leptogenesis can be realized at slightly lower values of v_R in the top left panel compared to the top right panel. However, a lower value of y_{33}^2 means radiative corrections to y_{i1} are smaller, so that slightly higher values of M_1 can be reached in the top right panel compared to the top left. Identical reasoning explains the slight variation in the bottom two panels when the active neutrinos obey a normal hierarchy.¹²

Last, Fig. 14 does not show the parameter region where radiative corrections to the mass of N_1 , (6.12), exceed M_1 . This is because the radiative corrections to M_1 are far less constraining than the radiative corrections to y_{i1} affecting the stability of N_1 . For example, when $\Lambda/v_R \leq 1$, $\Delta M_1 > M_1$ only when $v_R > 10^{13} \text{ GeV}$, which is not visible on Fig. 14. For larger values of Λ/v_R , the constraints from ΔM_1 do affect regions of parameter space for $v_R < 10^{13} \text{ GeV}$, but only for parameter space already excluded by the constraints from Δy_{i1} .

8.4 Natural leptogenesis for freeze-in cosmology

Just as neutrino mass relations tie together $g(x)$ and y_{33} in the freeze-out cosmology, so too do they tie $g(x)$ and y_{33} in the freeze-in cosmology, as is shown in Section 5.3. After requiring

¹¹ $m_2 = |m_2|$ since it is determined solely by the positive-definite dimension five mass contribution, $m_2^{(5)}$. m_3 is not necessarily positive because it may have a non-negligible see-saw contribution with a negative sign.

¹²A consistent neutrino mass spectrum requires $m_2 > m_3$ when $x \sim 1$, otherwise y_{33}^2 , a positive definite quantity, would be negative (see (8.7)). This is violated if $|m_2| < |m_3|$ and $m_3 > 0$, which is why this case is absent in Fig. 14.

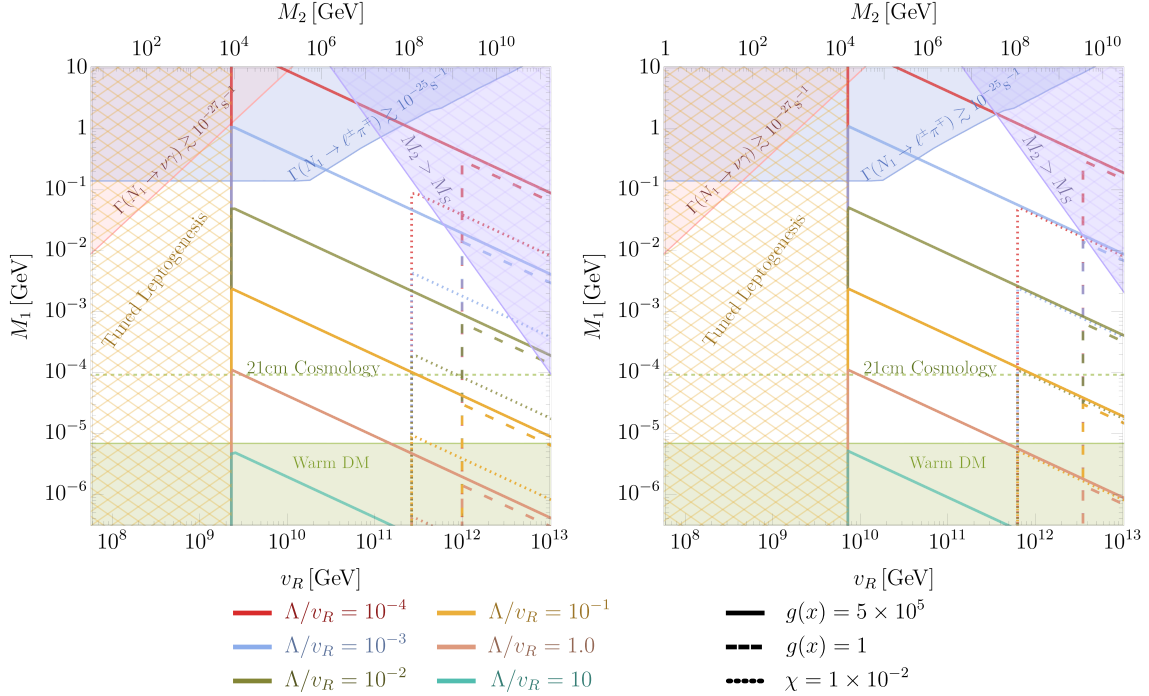


Figure 15. The parameter space where N_1 DM from freeze-in and N_2 leptogenesis can naturally be realized without radiative corrections affecting the stability of N_1 DM and in accord with the active neutrino mass spectrum. The unhatched shaded regions are constraints solely on N_1 DM from freeze-in as in Fig. 3. In the hatched **gold** region, the baryon asymmetry generated by N_2 , at the maximum possible $\eta Y_2 \simeq 0.1 Y_{\text{therm}}$, is unable to match the observed baryon asymmetry with $g(x)$ set to its largest natural value, and y_{33} constrained by neutrino masses. The right, downward sloping contours indicate where the radiative corrections to y_{i1} are sufficiently large that they must be unnaturally tuned with tree contributions to keep N_1 DM stable when $g(x)$ is set to its largest natural value, and y_{33} set by consistent neutrino masses. Each contour corresponds to a specific Λ/v_R , as shown by the legend at the bottom. The dashed and dotted contours show the same region when M_2 and M_3 are comparable, ($g(x) = 1$, dashed) and $m_3^{(ss)}$ and $m_3^{(5)}$ are as naturally degenerate as can be ($g(x)$ at χ_{min} , dotted). Naturalness and neutrino mass consistency excludes areas with too low or high values of v_R , and places a strong upper bound on the cutoff Λ . Regions with larger M_1 are only allowed if $\Lambda < v_R$, as occurs for the model of Sec. 7. The hatched **violet** region shows the inconsistent region where the mass of N_2 is greater than the mass of the heavy fermion that generates it. **Left:** We fix $m_{22} = \sqrt{\Delta m_{\text{atm}}^2}$ and $m_{33} = -\sqrt{\Delta m_{\text{atm}}^2 + \Delta m_{\text{sol}}^2}$ resembling the Inverted Hierarchy. Consequently, $m_{22}(m_{22} - m_{33}) \simeq (0.1 \text{ eV})^2$ and y_{33}^2 is relatively large at $x = 1$. **Right:** We fix $m_{22} = \sqrt{\Delta m_{\text{sol}}^2}$ and $m_{33} = -\sqrt{\Delta m_{\text{atm}}^2}$, resembling the Normal Hierarchy. Consequently, $m_{22}(m_{22} - m_{33}) \ll (0.1 \text{ eV})^2$ and y_{33}^2 is relatively small at $x = 1$.

$\tilde{m}_2 < 0.001$ eV to avoid strong wash-out, a similar relationship to (8.7) occurs:

$$y_{33}^2 \simeq (\sqrt{x} m_{22} - m_{33}) \sqrt{x} m_{22} \frac{v_R^2}{v^4}, \quad \left(\begin{array}{c} \text{Constraint from neutrino masses} \\ \text{in freeze-in cosmology} \end{array} \right) \quad (8.8)$$

where $|m_{33}| \lesssim 0.05$ eV and $m_{22} = M_2(v/v_R)^2 = 0.01 - 0.05$ eV.

In Fig. 15, we show the constraints on (v_R, M_1) when leptogenesis is incorporated naturally and consistently in the cosmology with N_1 DM from freeze-in. The shaded regions constraining N_1 DM remain from Fig. 3, but newly added is a hatched gold region where natural and consistent leptogenesis is inconsistent with the observed neutrino masses. Within the allowed region reside three triangles associated with the three familiar values of M_3/M_2 : $g(x)_{\max}$, solid; $g(x) = 1$, dashed; $g(x)$ at χ_{\min} , dotted. The right side of each triangle marks the region where y_{33} , as set by (8.8), is greater than y_{\max} , (6.10). The left side of the triangle, i.e. the boundary of the hatched gold region, marks the region where Y_B generated by N_2 , at the maximum possible $\eta Y_2 \simeq 0.1 Y_{\text{therm}}$, is unable to match the observed baryon asymmetry with y_{33} set by (8.8) and $\sin^2 \alpha \sin 2\beta = 1$. Within the unshaded region of each triangle, natural leptogenesis is possible for $\sin^2 \alpha \sin 2\beta < 1$. Each contour color corresponds to a different Λ/v_R spanning six decades from $10^{-4} - 10$, as shown by the legend at the bottom of the figure. Fig. 15 demonstrates that naturally reaching the highest masses of N_1 DM allowed in the freeze-in cosmology requires $\Lambda/v_R \ll 10^{-1}$.

The left side of the triangle in Fig. 15 is vertical unlike Fig. 14 because ηY_2 at its maximum is independent of M_1 due to the additional contribution from $Y_{\ell H}$. When $\tilde{m}_2 \not\sim 10^{-3}$ eV, $\eta Y_2 \leq 0.1 Y_{\text{therm}}$, and the triangular region shrinks (\tilde{m}_2 is defined in (5.6)). If $\tilde{m}_2 \ll 10^{-3}$, $Y_{\ell H} \ll Y_{W_R}$, and the left side of the triangular regions of Fig. 15 contract to match those of Fig. 14 for freeze-out.

Since m_{22} and m_{33} are unknown quantities generally misaligned with the active neutrino masses, it is impossible to know the exact parameter space associated with the normal and inverted hierarchies. Nevertheless, since m_{22} and $|m_{33}|$ remain of order the observed neutrino masses, the variations in the allowed parameter space do not change dramatically when scanning over possible values of m_{22} and m_{33} . For example, in the left panel of Fig. 15, $m_{22}(m_{22} - m_{33}) \simeq (0.1 \text{ eV})^2$ so that y_{33}^2 is at its largest when $x \sim 1$ for the same reasons discussed in Sec. 8.3 for freeze-out. In this case, leptogenesis can probe lower v_R due to the slight enhancement in y_{33} . In the right panel, $m_{22}(m_{22} - m_{33}) \ll (0.1 \text{ eV})^2$ so that y_{33}^2 is much smaller, and larger v_R is required to realize the observed baryon asymmetry. The right panel of Fig. 15 assumes m_{33} and m_{22} are not more degenerate than the observed neutrino mass spectrum. If they are significantly more degenerate, y_{33}^2 decreases and large v_R is required to generate the observed baryon asymmetry. Consequently, the naturally allowed triangular region shifts to higher v_R . Finally, the allowed region where $m_{22}(m_{22} - m_{33}) \lesssim (0.1 \text{ eV})^2$ lies between the triangular regions in the left and right panels of Fig. 15.

Within the hatched violet region, the mass of N_2 is greater than the mass of the heavy fermion, M_S , that generates it, which is inconsistent. This region is always more constraining

than the region where the reheat temperature after inflation, $T_{\text{RH}}^{\text{inf}}$, is below M_2 and leptogenesis becomes challenging. We do not analyze this region in this work.

Last, Fig. 15 does not show the region of parameter space where radiative corrections to the mass of N_1 , (6.12), are greater than M_1 for the same reasons discussed for the freeze-out cosmology: the radiative corrections to M_1 are weaker than the radiative corrections to y_{1i} and either do not show up on Fig. 15, or are already excluded by other means.

9 Conclusions and discussion

The discovery of the Higgs with a mass of 125 GeV has revealed that the Higgs quartic coupling nearly vanishes at a high energy scale ($10^9 - 10^{13}$) GeV. In extensions of the SM with a Z_2 symmetry called Higgs Parity, the spontaneous breaking of Higgs Parity yields the SM as a low energy effective theory. The SM Higgs quartic coupling is predicted to vanish at the Z_2 symmetry breaking scale, and hence precise measurements of SM parameters can narrow down the symmetry breaking scale. Observable quantities correlated with the symmetry breaking scale are correlated with SM parameters.

In this paper, we identified Higgs Parity with Left-Right symmetry, which is broken at scale v_R . By combining Left-Right Higgs Parity with space-time parity, the absence of CP violation in strong interactions is explained. Left-Right symmetry predicts three right-handed neutrinos. The lightest, N_1 , may be dark matter and the decay of a heavier one, N_2 , may create the baryon asymmetry of the universe through leptogenesis.

We studied two cosmological histories of the universe. In the freeze-out cosmology, the reheating temperature of the universe is high enough that right-handed neutrinos are initially thermalized via exchange of additional gauge bosons required by Left-Right symmetry. N_i later decouple from the thermal bath; N_1 are overproduced, but are diluted by the late-time decay of N_2 . N_2 decays also create the baryon asymmetry. In the freeze-in cosmology, the reheating temperature is low, so that the right-handed neutrinos are not thermalized, but an appropriate amount of N_1 is produced via new gauge boson exchange around the completion of reheating. N_2 are produced by the new gauge boson exchange and by Yukawa couplings to SM particles. The N_2 decays again produce the baryon asymmetry.

The freeze-out cosmology is tightly constrained. With quark and lepton masses generated by the effective theory of (2.4) and (2.5), successful dark matter and baryogenesis can be achieved simultaneously in the unshaded regions of the (v_R, M_1) plane of Fig. 4. The symmetry breaking scale is predicted to be $v_R = 10^8 - 10^{13}$ GeV; remarkably, this coincides with the window predicted from SM parameters and Higgs Parity. The parameter space can be probed by 21cm line cosmology and by precise measurements of SM parameters. If the effective theory has a UV completion below v_R , the allowed region is slightly enlarged, as shown in Fig. 11. The freeze-in cosmology, on the other hand, is consistent with simultaneous dark matter and baryogenesis over a wide range of (v_R, M_1) , including the entire unshaded region of Fig. 3.

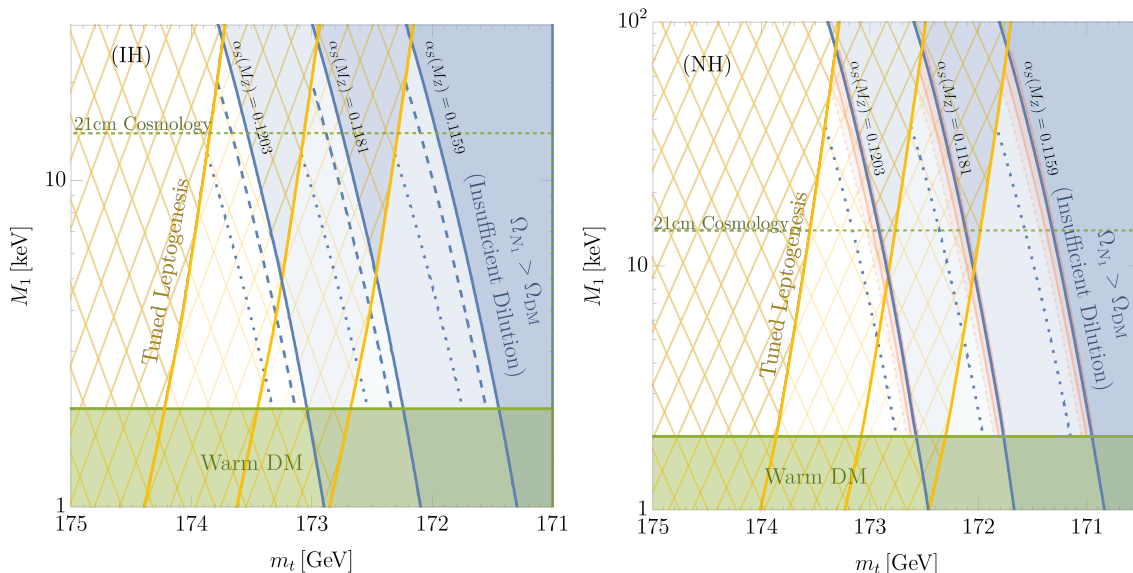


Figure 16. The parameter space of N_1 DM from freeze-out, natural leptogenesis, and consistent neutrino masses in terms of the mass of N_1 , M_1 , and the mass of the top quark, m_t . Remarkably, N_1 DM, natural leptogenesis, and the observed neutrino masses are consistent with the current measurement of $m_t = 173.0 \pm 0.4$ GeV. The center triangle fixes $\alpha_S(M_Z)$ at its central value, and the triangles to the left and right at $\pm 2\sigma$ values. We fix m_h at its central value throughout, since variations in m_h within its uncertainty do not appreciably change the parameter space. The ν_2 and ν_3 masses are fixed by: **Left** the Inverted Hierarchy (IH) in accordance with the top left panel of Fig. 14 and **Right** by the Normal Hierarchy (NH), in accordance with the bottom right panel of Fig. 14.

Naturalness of the scheme further constraints the parameter space as well as the origin of the fermion masses in the model. The stability of N_1 DM is not protected by any symmetry. Quantum corrections may induce Yukawa couplings of N_1 to the SM lepton doublets and Higgs, making N_1 decay too fast. We identified two types of quantum corrections. First, N_3 must have significant Yukawa couplings for efficient leptogenesis, while the tau Yukawa coupling explicitly breaks any symmetry that distinguishes N_3 from N_1 ; quantum corrections involving N_3 and tau Yukawa couplings destabilize N_1 . In some of the parameter space, to suppress these quantum corrections, the neutrino mass operators of (2.5) should be UV-completed by fields with a mass below v_R . Second, the $SU(2)_R$ doublet to which N_1 is embedded, $\bar{\ell}_1$, has Yukawa couplings to generate the charged lepton Yukawa couplings. The chiral symmetry of N_1 which can forbid its decay is explicitly broken by a combination of this Yukawa and the quark Yukawas. To suppress the resulting quantum corrections, the UV completion of the operators of (2.4), that generate charged fermion masses, requires fields with masses below v_R .

In most of parameter space, sufficient baryon asymmetry requires either the two heavier right-handed neutrinos $N_{2,3}$ are nearly degenerate, or the see-saw contribution to the SM neutrino masses from N_3 is nearly cancelled by a contribution from dimension-5 operators.

These two features can be explained naturally by UV models of the neutrino sector presented in Sec. 8.1. However, the near degeneracy or cancellation may be destabilized by quantum corrections, limiting the enhancement. This excludes lower values of v_R , where the masses of $N_{2,3}$ are small and significant enhancement of the CP asymmetry is required.

Constraints on the freeze-out cosmology, summarised in Fig. 14, allow $v_R \sim 10^{10} - 10^{13}(10^{12})$ GeV and $M_1 \sim 2-100(30)$ keV for the normal (inverted) hierarchy of SM neutrinos, respectively. Measurements of SM parameters, the warmness of DM, and the hierarchy of SM neutrinos can probe this parameter space. For example, if an inverted hierarchy is confirmed, $v_R < 10^{12}$ GeV is required, giving precise predictions for future measurements of m_t and α_s . Also, observations of cosmic 21cm line radiation will discover DM to be warm, unless $v_R \sim 10^{11}$ GeV. For a normal hierarchy, a wider range of v_R is allowed, but discovery or constraints on the warmness of DM will narrow down v_R , and hence SM parameters. If the CP asymmetry of leptogenesis is not enhanced by either degeneracy or cancellation, v_R and M_1 are required to be above 10^{12} GeV and around a few keV, respectively. This parameter region can be probed by measurements of SM parameters and the warmness of DM.

In Fig. 16, we recast the constraints on the (m_t, M_1) plane for a fixed Higgs mass and several values of a strong coupling constant. In Higgs Parity, the scale v_R depends dominantly on m_t , and to a lesser extent, $\alpha_S(M_Z)$ and the Higgs mass, m_h (see e.g. Fig. 1). Consequently, for fixed $\alpha_S(M_Z)$ and m_h , m_t acts as a direct substitute for the scale v_R . The allowed parameter space is in remarkable agreement with the observed top quark mass. Future measurements of m_t , $\alpha_S(M_Z)$, and m_h will hone in on the scale v_R and, together with determination of the neutrino mass hierarchy, will narrow the allowed range of M_1 . This can then be confirmed or excluded by 21 cm line cosmology. Here we assume that the running of gauge coupling constants is that of the SM up to the scale v_R . If the Dirac mass terms in Eqs. (7.9) and (7.15) are smaller than v_R , the running is slightly altered. If all of the Dirac masses are smaller than $y^{u,d,e}v_R$, there exists a set of new particles with masses $y^{u,d,e}v_R$. Even for this extreme case, the prediction for v_R for given SM parameters is increased only by a factor of two. For fixed v_R , this corresponds to an increase in the prediction for the top quark mass by 150 MeV. If the Dirac masses of fermions generating the first generation Yukawas are above v_R , the increase in v_R is at most only 10%. The corresponding increase in the top quark mass is 20 MeV, which is smaller than the expected uncertainty of top quark mass measurements at future lepton colliders [77–80].

In the freeze-out cosmology, if N_2 decays dominantly via W_R , a component of hot dark matter is predicted due to the subdominant decay mode $N_2 \rightarrow N_1 \ell^+ \ell^-$. This is a very natural possibility, occurring whenever the N_2 Yukawa couplings are sufficiently small. In this case the prediction for v_R , or equivalently m_t , is sharpened, corresponding to the right-hand blue side of the allowed regions in Fig. 16. The branching ratio of the decay into ℓH , which creates lepton asymmetry, is less than unity, but this can be compensated by the enhancement of the CP asymmetry. When charged fermion masses arise from the effective theory of (2.4), this hot component provides 10% of dark matter. However, in the case of UV completions discussed in Sec. 7, for a normal neutrino mass hierarchy too much hot dark matter is produced if N_2

decays dominantly via W_R , while for the inverted hierarchy the hot fraction is only 0.7%. The relevant N_2 branching ratios can be computed because the lepton flavor mixing matrix for W_R is the complex conjugate of the PMNS matrix.

The freeze-in cosmology is also constrained, as shown in Fig. 15; v_R must be above 10^9 GeV. If the CP asymmetry of leptogenesis is not enhanced by degeneracy or cancellation, v_R is required to be above 10^{12} GeV, constraining the parameters.

Theories of Higgs Parity suffer from the domain wall problem [81] if the Higgs Parity symmetry breaking occurs after inflation. To avoid the problem requires that the reheating temperature is at most v_R ; the constraint is typically stronger since the maximal temperature of the universe is in general higher than the reheating temperature [70, 82, 83] (see, however, [84]). As we have shown in this paper, the baryon asymmetry can be produced naturally via leptogenesis with the reheating temperature much smaller than v_R , especially in the freeze-in cosmology, safely avoiding the domain wall problem.

We conclude the paper by stressing the importance of cosmology and precise measurements for Higgs Parity. New physics scales in theories of Higgs Parity are high. New particles are heavy and/or very weakly coupled to SM particles. Direct confirmation of these theories by discovery of new particles or deviation from SM predictions at collider experiments will be difficult in the near future. In testing such theories, theoretical considerations on the early universe, cosmological observations, and predictions of SM parameters (including those of neutrinos) play key roles. In this paper, we investigated the production of dark matter and baryon densities in a Left-Right symmetric Higgs Parity theory. The theory can be in fact probed by the warmness of DM, precise determination of SM parameters by future colliders and lattice computations, and by the measurement of the neutrino hierarchy.

Acknowledgement

This work was supported in part by the Director, Office of Science, Office of High Energy and Nuclear Physics, of the US Department of Energy under Contracts DE-AC02-05CH11231 (LJH) and DE-SC0009988 (KH), by the National Science Foundation under grants PHY-1316783 and PHY-1521446 (LJH), as well as by the Raymond and Beverly Sackler Foundation Fund (KH).

References

- [1] ATLAS collaboration, *Observation of a new particle in the search for the Standard Model Higgs boson with the ATLAS detector at the LHC*, *Phys. Lett. B* **716** (2012) 1 [[1207.7214](#)].
- [2] CMS collaboration, *Observation of a New Boson at a Mass of 125 GeV with the CMS Experiment at the LHC*, *Phys. Lett. B* **716** (2012) 30 [[1207.7235](#)].
- [3] M. Redi and A. Strumia, *Axion-Higgs Unification*, *JHEP* **11** (2012) 103 [[1208.6013](#)].
- [4] L. J. Hall and Y. Nomura, *Grand Unification and Intermediate Scale Supersymmetry*, *JHEP* **02** (2014) 129 [[1312.6695](#)].

- [5] M. Ibe, S. Matsumoto and T. T. Yanagida, *Flat Higgs Potential from Planck Scale Supersymmetry Breaking*, *Phys. Lett.* **B732** (2014) 214 [[1312.7108](#)].
- [6] L. J. Hall, Y. Nomura and S. Shirai, *Grand Unification, Axion, and Inflation in Intermediate Scale Supersymmetry*, *JHEP* **06** (2014) 137 [[1403.8138](#)].
- [7] P. J. Fox, G. D. Kribs and A. Martin, *Split Dirac Supersymmetry: An Ultraviolet Completion of Higgsino Dark Matter*, *Phys. Rev.* **D90** (2014) 075006 [[1405.3692](#)].
- [8] L. J. Hall and K. Harigaya, *Implications of Higgs Discovery for the Strong CP Problem and Unification*, *JHEP* **10** (2018) 130 [[1803.08119](#)].
- [9] D. Dunsky, L. J. Hall and K. Harigaya, *Higgs Parity, Strong CP, and Dark Matter*, *JHEP* **07** (2019) 016 [[1902.07726](#)].
- [10] D. Dunsky, L. J. Hall and K. Harigaya, *Dark Matter, Dark Radiation and Gravitational Waves from Mirror Higgs Parity*, *JHEP* **02** (2020) 078 [[1908.02756](#)].
- [11] J. C. Pati and A. Salam, *Lepton Number as the Fourth Color*, *Phys. Rev. D* **10** (1974) 275.
- [12] R. Mohapatra and J. C. Pati, *A Natural Left-Right Symmetry*, *Phys. Rev. D* **11** (1975) 2558.
- [13] G. Senjanovic and R. N. Mohapatra, *Exact Left-Right Symmetry and Spontaneous Violation of Parity*, *Phys. Rev. D* **12** (1975) 1502.
- [14] L. J. Hall and K. Harigaya, *Higgs Parity Grand Unification*, *JHEP* **11** (2019) 033 [[1905.12722](#)].
- [15] K. S. Babu and R. N. Mohapatra, *A Solution to the Strong CP Problem Without an Axion*, *Phys. Rev.* **D41** (1990) 1286.
- [16] R. D. Peccei and H. R. Quinn, *CP Conservation in the Presence of Instantons*, *Phys. Rev. Lett.* **38** (1977) 1440.
- [17] R. D. Peccei and H. R. Quinn, *Constraints Imposed by CP Conservation in the Presence of Instantons*, *Phys. Rev.* **D16** (1977) 1791.
- [18] S. Weinberg, *A New Light Boson?*, *Phys. Rev. Lett.* **40** (1978) 223.
- [19] F. Wilczek, *Problem of Strong P and T Invariance in the Presence of Instantons*, *Phys. Rev. Lett.* **40** (1978) 279.
- [20] J. Preskill, M. B. Wise and F. Wilczek, *Cosmology of the Invisible Axion*, *Phys. Lett.* **120B** (1983) 127.
- [21] L. F. Abbott and P. Sikivie, *A Cosmological Bound on the Invisible Axion*, *Phys. Lett.* **120B** (1983) 133.
- [22] M. Dine and W. Fischler, *The Not So Harmless Axion*, *Phys. Lett.* **120B** (1983) 137.
- [23] P. Sikivie, *Of Axions, Domain Walls and the Early Universe*, *Phys. Rev. Lett.* **48** (1982) 1156.
- [24] R. L. Davis, *Cosmic Axions from Cosmic Strings*, *Phys. Lett. B* **180** (1986) 225.
- [25] M. Kawasaki, K. Saikawa and T. Sekiguchi, *Axion dark matter from topological defects*, *Phys. Rev. D* **91** (2015) 065014 [[1412.0789](#)].
- [26] R. T. Co, L. J. Hall and K. Harigaya, *QCD Axion Dark Matter with a Small Decay Constant*, *Phys. Rev. Lett.* **120** (2018) 211602 [[1711.10486](#)].

- [27] R. T. Co, L. J. Hall and K. Harigaya, *Axion Kinetic Misalignment Mechanism*, *Phys. Rev. Lett.* **124** (2020) 251802 [[1910.14152](#)].
- [28] T. Yanagida, *Horizontal gauge symmetry and masses of neutrinos*, *Conf. Proc.* **C7902131** (1979) 95.
- [29] M. Gell-Mann, P. Ramond and R. Slansky, *Complex Spinors and Unified Theories*, *Conf. Proc.* **C790927** (1979) 315 [[1306.4669](#)].
- [30] P. Minkowski, *$\mu \rightarrow e\gamma$ at a Rate of One Out of 10^9 Muon Decays?*, *Phys. Lett.* **67B** (1977) 421.
- [31] R. N. Mohapatra and G. Senjanovic, *Neutrino Mass and Spontaneous Parity Nonconservation*, *Phys. Rev. Lett.* **44** (1980) 912.
- [32] M. Fukugita and T. Yanagida, *Baryogenesis Without Grand Unification*, *Phys. Lett. B* **174** (1986) 45.
- [33] S. Khalil and O. Seto, *Sterile neutrino dark matter in $B - L$ extension of the standard model and galactic 511-keV line*, *JCAP* **10** (2008) 024 [[0804.0336](#)].
- [34] F. Bezrukov, H. Hettmansperger and M. Lindner, *keV sterile neutrino Dark Matter in gauge extensions of the Standard Model*, *Phys. Rev.* **D81** (2010) 085032 [[0912.4415](#)].
- [35] J. A. Dror, D. Dunsky, L. J. Hall and K. Harigaya, *Sterile Neutrino Dark Matter in Left-Right Theories*, [2004.09511](#).
- [36] M. A. B. Beg and H. S. Tsao, *Strong P , T Noninvariances in a Superweak Theory*, *Phys. Rev. Lett.* **41** (1978) 278.
- [37] R. N. Mohapatra and G. Senjanovic, *Natural Suppression of Strong p and t Noninvariance*, *Phys. Lett.* **79B** (1978) 283.
- [38] R. Kuchimanchi, *Solution to the strong CP problem: Supersymmetry with parity*, *Phys. Rev. Lett.* **76** (1996) 3486 [[hep-ph/9511376](#)].
- [39] R. N. Mohapatra and A. Rasin, *Simple supersymmetric solution to the strong CP problem*, *Phys. Rev. Lett.* **76** (1996) 3490 [[hep-ph/9511391](#)].
- [40] K. S. Babu and R. N. Mohapatra, *CP Violation in Seesaw Models of Quark Masses*, *Phys. Rev. Lett.* **62** (1989) 1079.
- [41] D. Buttazzo, G. Degrandi, P. P. Giardino, G. F. Giudice, F. Sala, A. Salvio et al., *Investigating the near-criticality of the Higgs boson*, *JHEP* **12** (2013) 089 [[1307.3536](#)].
- [42] S. Dodelson and L. M. Widrow, *Sterile-neutrinos as dark matter*, *Phys. Rev. Lett.* **72** (1994) 17 [[hep-ph/9303287](#)].
- [43] M. Drewes et al., *A White Paper on keV Sterile Neutrino Dark Matter*, *JCAP* **1701** (2017) 025 [[1602.04816](#)].
- [44] K. Nandra et al., *The Hot and Energetic Universe: A White Paper presenting the science theme motivating the Athena+ mission*, [1306.2307](#).
- [45] V. Tatischeff et al., *The e-ASTROGAM gamma-ray space mission*, *Proc. SPIE Int. Soc. Opt. Eng.* **9905** (2016) 99052N [[1608.03739](#)].
- [46] A. Caputo, M. Regis and M. Taoso, *Searching for Sterile Neutrino with X-ray Intensity Mapping*, *JCAP* **2003** (2020) 001 [[1911.09120](#)].

- [47] R. Essig, E. Kuflik, S. D. McDermott, T. Volansky and K. M. Zurek, *Constraining Light Dark Matter with Diffuse X-Ray and Gamma-Ray Observations*, *JHEP* **11** (2013) 193 [[1309.4091](#)].
- [48] L. Lavoura, *General formulae for $f(1) \rightarrow f(2)$ gamma*, *Eur. Phys. J. C* **29** (2003) 191 [[hep-ph/0302221](#)].
- [49] A. Greljo, D. J. Robinson, B. Shakya and J. Zupan, *$R(D^{(*)})$ from W' and right-handed neutrinos*, *JHEP* **09** (2018) 169 [[1804.04642](#)].
- [50] S. Tremaine and J. E. Gunn, *Dynamical Role of Light Neutral Leptons in Cosmology*, *Phys. Rev. Lett.* **42** (1979) 407.
- [51] A. Boyarsky, O. Ruchayskiy and D. Iakubovskiy, *A Lower bound on the mass of Dark Matter particles*, *JCAP* **0903** (2009) 005 [[0808.3902](#)].
- [52] D. Gorbunov, A. Khmelitsky and V. Rubakov, *Constraining sterile neutrino dark matter by phase-space density observations*, *JCAP* **0810** (2008) 041 [[0808.3910](#)].
- [53] V. K. Narayanan, D. N. Spergel, R. Dave and C.-P. Ma, *Constraints on the mass of warm dark matter particles and the shape of the linear power spectrum from the Ly α forest*, *Astrophys. J.* **543** (2000) L103 [[astro-ph/0005095](#)].
- [54] V. Irsic et al., *New Constraints on the free-streaming of warm dark matter from intermediate and small scale Lyman- α forest data*, *Phys. Rev.* **D96** (2017) 023522 [[1702.01764](#)].
- [55] C. Yèche, N. Palanque-Delabrouille, J. Baur and H. du Mas des Bourboux, *Constraints on neutrino masses from Lyman-alpha forest power spectrum with BOSS and XQ-100*, *JCAP* **1706** (2017) 047 [[1702.03314](#)].
- [56] U. Seljak, A. Makarov, P. McDonald and H. Trac, *Can sterile neutrinos be the dark matter?*, *Phys. Rev. Lett.* **97** (2006) 191303 [[astro-ph/0602430](#)].
- [57] T. Asaka, M. Shaposhnikov and A. Kusenko, *Opening a new window for warm dark matter*, *Phys. Lett.* **B638** (2006) 401 [[hep-ph/0602150](#)].
- [58] K. Harigaya and M. Kawasaki, *QCD axion dark matter from long-lived domain walls during matter domination*, *Phys. Lett.* **B782** (2018) 1 [[1802.00579](#)].
- [59] M. Kawasaki, K. Kohri and N. Sugiyama, *Cosmological constraints on late time entropy production*, *Phys. Rev. Lett.* **82** (1999) 4168 [[astro-ph/9811437](#)].
- [60] M. Kawasaki, K. Kohri and N. Sugiyama, *MeV scale reheating temperature and thermalization of neutrino background*, *Phys. Rev.* **D62** (2000) 023506 [[astro-ph/0002127](#)].
- [61] T. Hasegawa, N. Hiroshima, K. Kohri, R. S. Hansen, T. Tram and S. Hannestad, *MeV-scale reheating temperature and thermalization of oscillating neutrinos by radiative and hadronic decays of massive particles*, *JCAP* **12** (2019) 012 [[1908.10189](#)].
- [62] K. Ichikawa, M. Kawasaki and F. Takahashi, *The Oscillation effects on thermalization of the neutrinos in the Universe with low reheating temperature*, *Phys. Rev.* **D72** (2005) 043522 [[astro-ph/0505395](#)].
- [63] P. F. de Salas, M. Lattanzi, G. Mangano, G. Miele, S. Pastor and O. Pisanti, *Bounds on very low reheating scenarios after Planck*, *Phys. Rev.* **D92** (2015) 123534 [[1511.00672](#)].
- [64] J. B. Muoz, C. Dvorkin and F.-Y. Cyr-Racine, *Probing the Small-Scale Matter Power Spectrum with Large-Scale 21-cm Data*, *Phys. Rev. D* **101** (2020) 063526 [[1911.11144](#)].

- [65] L. Feng, J.-F. Zhang and X. Zhang, *A search for sterile neutrinos with the latest cosmological observations*, *Eur. Phys. J. C* **77** (2017) 418 [[1703.04884](#)].
- [66] CMB-S4 collaboration, *CMB-S4 Science Book, First Edition*, [1610.02743](#).
- [67] K. Abazajian et al., *CMB-S4 Science Case, Reference Design, and Project Plan*, [1907.04473](#).
- [68] J. Heeck and D. Teresi, *Cold keV dark matter from decays and scatterings*, *Phys. Rev.* **D96** (2017) 035018 [[1706.09909](#)].
- [69] J. A. Harvey and M. S. Turner, *Cosmological baryon and lepton number in the presence of electroweak fermion number violation*, *Phys. Rev.* **D42** (1990) 3344.
- [70] E. W. Kolb and M. S. Turner, *The Early Universe*, vol. 69. 1990.
- [71] R. T. Co, F. D’Eramo, L. J. Hall and D. Pappadopulo, *Freeze-In Dark Matter with Displaced Signatures at Colliders*, *JCAP* **1512** (2015) 024 [[1506.07532](#)].
- [72] G. F. Giudice, A. Notari, M. Raidal, A. Riotto and A. Strumia, *Towards a complete theory of thermal leptogenesis in the SM and MSSM*, *Nucl. Phys.* **B685** (2004) 89 [[hep-ph/0310123](#)].
- [73] L. Covi, E. Roulet and F. Vissani, *CP violating decays in leptogenesis scenarios*, *Phys. Lett. B* **384** (1996) 169 [[hep-ph/9605319](#)].
- [74] S. Davidson, E. Nardi and Y. Nir, *Leptogenesis*, *Phys. Rept.* **466** (2008) 105 [[0802.2962](#)].
- [75] X.-D. Shi and G. M. Fuller, *A New dark matter candidate: Nonthermal sterile neutrinos*, *Phys. Rev. Lett.* **82** (1999) 2832 [[astro-ph/9810076](#)].
- [76] I. Esteban, M. Gonzalez-Garcia, A. Hernandez-Cabezudo, M. Maltoni and T. Schwetz, *Global analysis of three-flavour neutrino oscillations: synergies and tensions in the determination of θ_{23} , δ_{CP} , and the mass ordering*, *JHEP* **01** (2019) 106 [[1811.05487](#)].
- [77] K. Seidel, F. Simon, M. Tesar and S. Poss, *Top quark mass measurements at and above threshold at CLIC*, *Eur. Phys. J. C* **73** (2013) 2530 [[1303.3758](#)].
- [78] T. Horiguchi, A. Ishikawa, T. Suehara, K. Fujii, Y. Sumino, Y. Kiyo et al., *Study of top quark pair production near threshold at the ILC*, [1310.0563](#).
- [79] Y. Kiyo, G. Mishima and Y. Sumino, *Strong IR Cancellation in Heavy Quarkonium and Precise Top Mass Determination*, *JHEP* **11** (2015) 084 [[1506.06542](#)].
- [80] M. Beneke, Y. Kiyo, P. Marquard, A. Penin, J. Piclum and M. Steinhauser, *Next-to-Next-to-Next-to-Leading Order QCD Prediction for the Top Antitop S-Wave Pair Production Cross Section Near Threshold in e^+e^- Annihilation*, *Phys. Rev. Lett.* **115** (2015) 192001 [[1506.06864](#)].
- [81] Y. Zeldovich, I. Kobzarev and L. Okun, *Cosmological Consequences of the Spontaneous Breakdown of Discrete Symmetry*, *Zh. Eksp. Teor. Fiz.* **67** (1974) 3.
- [82] K. Harigaya and K. Mukaida, *Thermalization after/during Reheating*, *JHEP* **05** (2014) 006 [[1312.3097](#)].
- [83] K. Mukaida and M. Yamada, *Thermalization Process after Inflation and Effective Potential of Scalar Field*, *JCAP* **02** (2016) 003 [[1506.07661](#)].
- [84] R. T. Co, E. Gonzalez and K. Harigaya, *Increasing Temperature toward the Completion of Reheating*, [2007.04328](#).